

Probing triaxial deformation of atomic nuclei in high-energy heavy ion collisions

Jiangyong Jia^{1,2,*}

¹*Department of Chemistry, Stony Brook University, Stony Brook, NY 11794, USA*

²*Physics Department, Brookhaven National Laboratory, Upton, NY 11976, USA*

(Dated: April 14, 2022)

Most atomic nuclei are deformed with a quadrupole shape described by its overall strength β_2 and triaxiality γ . The deformation can be accessed in high-energy heavy-ion collisions by measuring the collective flow response of the produced quark-gluon plasma to the eccentricity ε_2 and the density gradient d_\perp in the initial state. Using an analytical estimate and a Glauber model, I show that the variances, $\langle \varepsilon_2^2 \rangle$ or $\langle (\delta d_\perp / d_\perp)^2 \rangle$, and skewnesses, $\langle \varepsilon_2^3 \delta d_\perp / d_\perp \rangle$ or $\langle (\delta d_\perp / d_\perp)^3 \rangle$, have a simple analytical form of $a' + b'\beta_2^2$ and $a' + (b' + c' \cos(3\gamma))\beta_2^3$, respectively. From these, I constructed several normalized skewnesses to isolate the γ dependence from that of β_2 , and show that the correlations between a normalized skewness and a variance can constrain simultaneously the β_2 and γ . Assuming a linear relation with elliptic flow v_2 and mean-transverse momentum $[p_T]$ of final-state particles, $v_2 \propto \varepsilon_2$ and $\delta[p_T]/[p_T] \propto \delta d_\perp / d_\perp$, similar conclusions are also expected for the variances and skewnesses of v_2 and $[p_T]$, i.e. $a + b\beta_2^2$ for $\langle v_2^2 \rangle$ and $\langle (\delta[p_T]/[p_T])^2 \rangle$ and $a + (b + c \cos(3\gamma))\beta_2^3$ for $\langle v_2^3 \delta[p_T]/[p_T] \rangle$ or $\langle (\delta[p_T]/[p_T])^3 \rangle$. These findings motivate a dedicated system scan of high-energy heavy-ion collisions at RHIC and LHC to measure triaxiality of atomic nuclei: one first determines the coefficients b and c by collisions of isobaric near prolate nuclei, $\cos(3\gamma) \approx 1$, and near oblate nuclei, $\cos(3\gamma) \approx -1$, with known β_2 values, followed by collisions of other species of interest with similar mass number. The (β_2, γ) values for this species can be inferred directly from the measured variance and skewness observables from these collisions. The results demonstrate the unique opportunities offered by high-energy collisions as a tool to perform interdisciplinary nuclear physics studies.

PACS numbers: 25.75.Gz, 25.75.Ld, 25.75.-1

I. INTRODUCTION

Most atomic nuclei in their ground state are deformed from a well-defined spherical shape. Nuclear deformation arises due to short-range strong nuclear force among nucleons themselves, and depending on the proton and neutron number, the minima in the total energy of the system can be found for spherical, ellipsoidal, octuple and hexadecapole shapes [1–5]. Information about nuclear deformation is primarily extracted from spectroscopic measurements and models of reduced transition probability $B(E\lambda)$ between low-lying rotational states, which involves nuclear experiments with energy per nucleon less than few tens of MeVs. Recently, the prospects of probing the nuclear deformation at much higher beam energy, energy per nucleon exceeding hundreds of GeVs, by taking advantage of the hydrodynamic flow behavior of large number of produced final-state particles, have been discussed [6–16], and evidence from several experiments has been observed [17–21].

The shape of a nucleus, including only the dominant quadrupole component, is often described by a nuclear density profile of the Woods-Saxon form,

$$\rho(r, \theta, \phi) = \frac{\rho_0}{1 + e^{[r - R(\theta, \phi)]/a}}, \quad R(\theta, \phi) = R_0 (1 + \beta_2 [\cos \gamma Y_{2,0}(\theta, \phi) + \sin \gamma Y_{2,2}(\theta, \phi)]), \quad (1)$$

where the nuclear surface $R(\theta, \phi)$ is expanded into real form spherical harmonics $Y_{2,m}$ in the intrinsic frame. The positive number β_2 describes the overall quadrupole deformation, and the triaxiality parameter γ controls the relative order of the three radii r_a, r_b, r_c of the nucleus in the intrinsic frame. It has the range $0 \leq \gamma \leq \pi/3$, with $\gamma = 0$, $\gamma = \pi/3$, and $\gamma = \pi/6$ corresponding, respectively, to prolate ($r_a = r_b < r_c$), oblate ($r_a < r_b = r_c$) or rigid triaxiality ($r_a < r_b < r_c$ and $2r_b = r_a + r_c$), see top row of Fig. 1 for an illustration. Most nuclei have axially symmetric prolate or oblate shapes, and triaxiality is a rather elusive signature in nuclear structure physics. The triaxial degree of freedom is related to a number of interesting phenomena including the γ -band [22], chirality [23] and wobbling motion [24, 25], but the extraction of γ value has significant experimental and theoretical uncertainties. An interesting question is if and how triaxiality may manifest itself in other fields of nuclear physics.

High-energy heavy-ion collisions at RHIC and the LHC, especially head-on collisions with nearly zero impact parameter (ultracentral collisions or UCC), provide a new way to image the shape of the nucleus. The large amount

* Correspond to jiangyong.jia@stonybrook.edu

of energy deposited in these collisions leads to the formation of a hot and dense quark-gluon plasma (QGP) [26] in the overlap region, whose shape and size are strongly correlated with nuclear deformation as illustrated by the second row of Fig. 1. The transverse area S_{\perp} (or size R_{\perp}) and eccentricity of the overlap can be quantified by

$$S_{\perp} \equiv \pi R_{\perp}^2 = \pi \sqrt{\langle x^2 \rangle \langle y^2 \rangle}, \quad \epsilon_2 \equiv \varepsilon_2 e^{i2\Phi_2} = -\frac{\langle r_{\perp}^2 e^{i2\phi} \rangle}{\langle r_{\perp}^2 \rangle}, \quad (2)$$

where the average is over nucleons in the transverse plane $(x, y) = (r_{\perp}, \phi)$ in the rotated center-of-mass frame such that x (y) corresponds to the minor (major) axis of the ellipsoid. Within the liquid-drop model with a sharp surface, the variances of ε_2 and R_{\perp} over many head-on collisions are directly related to the β_2 : $\langle \varepsilon_2^2 \rangle = \frac{3}{2\pi} \beta_2^2$, $\langle (\delta R_{\perp}/R_{\perp})^2 \rangle = -\frac{1}{16\pi} \beta_2^2$, where $\delta R_{\perp}/R_{\perp} \equiv (R_{\perp} - \langle R_{\perp} \rangle)/\langle R_{\perp} \rangle$ denotes the event-by-event fluctuations relative to the average. Driven by the large pressure gradient forces and subsequent hydrodynamic collective expansion, the initial shape and size information is transferred into azimuthal and radial flow of final-state hadrons [27]. Specifically, the particle momentum spectra in each collision event can be parametrized as $\frac{d^2N}{p_T dp_T d\phi} = N(p_T) [1 + 2v_2(p_T) \cos 2(\phi - \Psi)]$ in ϕ and transverse momentum p_T . The magnitude of the radial flow, characterized by the slope of the particle spectrum $N(p_T)$ or the average $[p_T]$, is positively correlated with the gradient of nucleon density or inverse transverse size d_{\perp}

$$d_{\perp} = \sqrt{N_{\text{part}}/S_{\perp}}, \quad (3)$$

in the overlap region [28, 29], with N_{part} being the number of participating nucleons. This is because $d_{\perp} \propto 1/R_{\perp}$ is proportional to the pressure gradient and therefore is expected to be correlated with $[p_T]$. Similarly, the amplitude and orientation of elliptic flow, characterized by $V_2 = v_2 e^{i2\Psi}$, is directly related to $\epsilon_2 = \varepsilon_2 e^{i2\Phi}$. In fact, detailed hydrodynamic model simulations [29, 30] show good linear relations, for events with fixed N_{part} .

$$v_2 = k_2 \varepsilon_2, \quad \frac{\delta[p_T]}{[p_T]} = k_0 \frac{\delta d_{\perp}}{d_{\perp}} = -k_0 \frac{\delta R_{\perp}}{R_{\perp}} = -k_0 \frac{1}{2} \frac{\delta S_{\perp}}{S_{\perp}}. \quad (4)$$

The response coefficients k_2 and k_0 capture the transport properties of the QGP and they have been constrained theoretically [31–34].

As indicated clearly in the second row of Fig. 1, in ultracentral collisions of prolate nuclei, the shape of overlap falls in between “body-body” and “tip-tip” configurations with the long-axis perpendicular or parallel to the beam, respectively. The body-body collisions have large ε_2 and larger size R_{\perp} and therefore smaller d_{\perp} , while the tip-tip collisions have near-zero ε_2 and larger d_{\perp} , i.e. the correlation of ε_2 and d_{\perp} is negative $\langle \varepsilon_2^2 \delta d_{\perp} \rangle < 0$ [35]. In contrast, the covariance of ε_2 and d_{\perp} is expected to be positive for collisions of oblate nuclei, and zero for collisions of rigid triaxial nuclei [14]. Eq. (4) would then imply that $\langle v_2^2 \delta[p_T] \rangle < 0, > 0$ and $= 0$ for collisions of prolate, oblate and rigid triaxial nuclei, respectively. In fact, one finds that both $\langle \varepsilon_2^2 \delta d_{\perp} \rangle$ and $\langle v_2^2 \delta[p_T] \rangle$ are dominated by a $\cos(3\gamma)$ dependence in the ultracentral collisions, not surprising given the three-fold symmetry of nuclear shape in the γ angle.

Another interesting aspect of the deformation in heavy ion collisions, not discussed yet in the literature, concerns the nature of the event-by-event fluctuations of R_{\perp} or d_{\perp} in the presence of deformation and how they influence the $[p_T]$ fluctuations. As shown in the bottom row of Fig. 1, the probability for various overlap configurations are not equal. In collisions of rigid triaxial nuclei, the shape of the overlap in the transverse plane falls in between three configurations for the two axes of the ellipse: “ $r_b - r_a$ ”, “ $r_c - r_a$ ” and “ $r_c - r_b$ ”. The combination “ $r_c - r_a$ ” has the largest probability, and as the nucleus becomes more prolate (oblate), the middle branch merges with the right (left) branch and the distribution becomes more asymmetric. This gives rise to a nonvanishing skewness $\langle (\delta d_{\perp})^3 \rangle \sim -\langle (\delta R_{\perp})^3 \rangle$, and the sign of $\langle (\delta d_{\perp})^3 \rangle$ is expected to be opposite to that of $\langle \varepsilon_2^2 \delta d_{\perp} \rangle$. Indeed, one finds that $\langle (\delta d_{\perp})^3 \rangle$ contains a large $\cos(3\gamma)$ term, which is expected to drive a similar term for the skewness $\langle (\delta[p_T])^3 \rangle$ in the final state. Therefore, I have identified two three-particle correlation observables, $\langle v_2^2 \delta[p_T] \rangle$ and $\langle (\delta[p_T])^3 \rangle$, to probe nuclear triaxiality in heavy ion collisions. The β_2 value on the other hand can be constrained from two-particle correlation observables $\langle v_2^2 \rangle$ and $\langle (\delta[p_T])^2 \rangle$.

Several experimental studies of nuclear deformation in heavy ion collisions have been carried at RHIC [13, 17] and the LHC [18–20], focusing mostly on the relation between β_2 and v_2 in the UCC. However, the most striking evidence is provided by the recent measurement of $\langle v_2^2 \delta[p_T] \rangle$ and $\langle (\delta[p_T])^3 \rangle$ in $^{197}\text{Au} + ^{197}\text{Au}$ and $^{238}\text{U} + ^{238}\text{U}$ collisions at RHIC [21]. The large prolate deformation of ^{238}U yields a large negative contribution to $\langle v_2^2 \delta[p_T] \rangle$ and a large positive contribution to $\langle (\delta[p_T])^3 \rangle$, consistent with the picture in Fig. 1 discussed above. A few model studies on the feasibility of constraining triaxiality in heavy ion collisions appeared recently [14–16]. In light of these measurements and model work, I aim to clarify, via a Monte-Carlo Glauber model and a transport model, the influence of deformation on the cumulants of ε_2 and $[p_T]$. Remarkably, one finds that the β_2 and γ dependencies of these observables follow

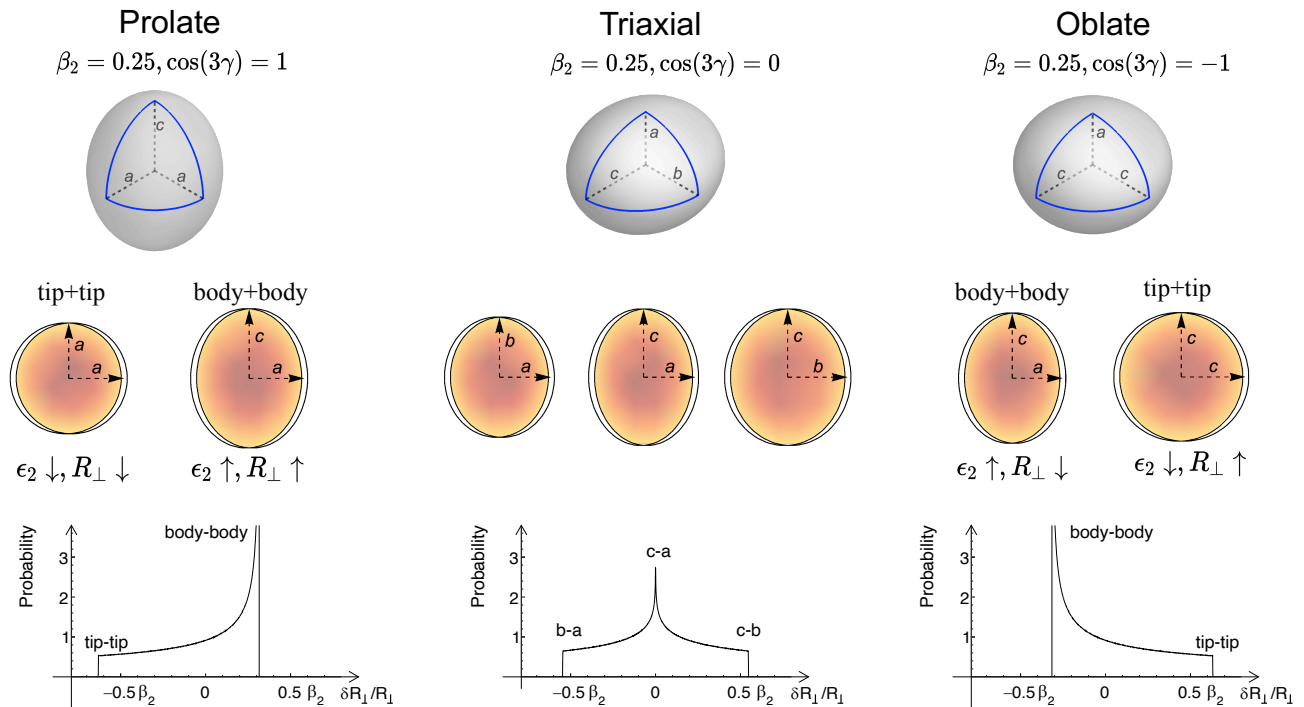


FIG. 1. The cartoon of a nucleus with quadrupole deformation $\beta_2 = 0.25$ (top row) with prolate (left), rigid triaxial (middle), and oblate (right) shape, the overlap containing the quark-gluon plasma in the ultracentral collisions (middle row) and distributions of the transverse size, $\delta R_\perp/R_1 = -\delta d_\perp/d_\perp$, derived from Eq. (11) (bottom row). The distributions in the bottom are given in units of β_2 .

very simple parametric functional forms. In particular, one finds that $\langle \epsilon_2^2 \rangle$ and $\langle \delta(d_\perp)^3 \rangle$ can be well described by a function of the $a' + b'\beta_2^2$ form, while $\langle \epsilon_2^2 \delta d_\perp \rangle$ and $\langle \delta(d_\perp)^3 \rangle$ by a function of the $a' + (b' + c' \cos(3\gamma))\beta_2^3$ form, with b' and c' nearly independent of the size of the collision systems. This finding provides a motivation for a collision system scan of nuclei at ultrarelativistic energies with similar β_2 but different γ values, which may provide additional insight on the question of shape evolution and shape coexistence [1] in low-energy nuclear structure physics.

II. SIMPLE ANALYTICAL ESTIMATE

I first predict the analytical form for the (β_2, γ) dependencies using a simple heuristic argument. For small deformation β_2 , the values of d_\perp and ϵ_2 in a given event are expected to have the following form:

$$\frac{\delta d_\perp}{d_\perp} = \delta_d + p_0(\Omega_1, \Omega_2, \gamma)\beta_2 + \mathcal{O}(\beta_2^2), \quad \epsilon_2 = \epsilon_0 + \mathbf{p}_2(\Omega_1, \Omega_2, \gamma)\beta_2 + \mathcal{O}(\beta_2^2), \quad (5)$$

where the scalar δ_d and vector $\epsilon_0 = \epsilon_0 e^{i2\Phi_{2,0}}$ are values for spherical nuclei, which in UCC collisions are dominated by random fluctuations of nucleons positions but in noncentral collisions are also affected by the impact-parameter-dependent average shape of the overlap. The p_0 and \mathbf{p}_2 are phase-space factors controlled by the Euler angles $\Omega = \phi\theta\psi$ of the two nuclei; they also contain the γ parameter. For example, in collision of prolate nuclei (see left of the middle row of Fig 1), $|p_0|$ and $|\mathbf{p}_2|$ are largest for the ‘‘body-body’’ orientation and smallest for the ‘‘tip-tip’’ orientation. Since the fluctuation of δ_d (ϵ_0) is uncorrelated with p_0 (\mathbf{p}_2), an average over collisions with different Euler angles is expect to give the following expression for the variances

$$C_d\{2\} \equiv \left\langle \left(\frac{\delta d_\perp}{d_\perp} \right)^2 \right\rangle = \langle \delta_d^2 \rangle + \langle p_0(\Omega_1, \Omega_2, \gamma)^2 \rangle \beta_2^2, \quad c_{2,\epsilon}\{2\} \equiv \langle \epsilon_2^2 \rangle = \langle \epsilon_0^2 \rangle + \langle \mathbf{p}_2(\Omega_1, \Omega_2, \gamma) \mathbf{p}_2^*(\Omega_1, \Omega_2, \gamma) \rangle \beta_2^2. \quad (6)$$

The $\langle p_0^2 \rangle$ and $\langle \mathbf{p}_2 \mathbf{p}_2^* \rangle$ are constants obtained by averaging over Ω_1 and Ω_2 . This argument can be generalized to higher-order cumulants. For example, the skewness and kurtosis of $p(d_\perp)$ and kurtosis of ϵ_2 can be written as,

$$\begin{aligned} C_d\{3\} &\equiv \left\langle \left(\frac{\delta d_\perp}{d_\perp} \right)^3 \right\rangle = \langle \delta_d^3 \rangle + \langle p_0^3 \rangle \beta_2^3, \\ C_d\{4\} &\equiv \left\langle \left(\frac{\delta d_\perp}{d_\perp} \right)^4 \right\rangle - 3 \left\langle \left(\frac{\delta d_\perp}{d_\perp} \right)^2 \right\rangle^2 = \langle \delta_d^4 \rangle - 3 \langle \delta_d^2 \rangle^2 + (\langle p_0^4 \rangle - 3 \langle p_0^2 \rangle^2) \beta_2^4 \\ c_{2,\epsilon}\{4\} &\equiv \langle \epsilon_2^4 \rangle - 2 \langle \epsilon_2^2 \rangle^2 = \langle \epsilon_0^4 \rangle - 2 \langle \epsilon_0^2 \rangle^2 + (\langle \mathbf{p}_2^2 \mathbf{p}_2^{*2} \rangle - 2 \langle \mathbf{p}_2 \mathbf{p}_2^* \rangle^2) \beta_2^4, \end{aligned} \quad (7)$$

where I use the fact that $\langle \mathbf{p}_2^n \mathbf{p}_2^{*m} \rangle = 0$ for $n \neq m$ due to the invariance under a global rotation. I shall skip the straightforward expression for higher-order cumulant of ϵ_2 . Another interesting example is mixed-skewness $\langle \epsilon_2^2 \frac{\delta d_\perp}{d_\perp} \rangle$, a good estimator for $\left\langle v_2^2 \frac{\delta[p_T]}{[p_T]} \right\rangle$,

$$\left\langle \epsilon_2^2 \frac{\delta d_\perp}{d_\perp} \right\rangle = \langle \epsilon_0^2 \delta_d \rangle + \langle p_0 \mathbf{p}_2 \mathbf{p}_2^* \rangle \beta_2^3. \quad (8)$$

Note that in noncentral collisions, the cross-term like $\langle p_0 (\mathbf{p}_2 \epsilon_0^* + \mathbf{p}_2^* \epsilon_0) \rangle \beta_2^2$ term may not vanish due to possible alignment between ϵ_0 and \mathbf{p}_2 .

This argument can be generalized to simultaneous presence of octuple or hexadecapole deformations for which additional axial symmetric components are added to the nuclear surface in Eq. (1),

$$R(\theta, \phi) = R_0 (1 + \beta_2 [\cos \gamma Y_{2,0}(\theta, \phi) + \sin \gamma Y_{2,2}(\theta, \phi)] + \beta_3 Y_{3,0}(\theta, \phi) + \beta_4 Y_{4,0}(\theta, \phi)), \quad (9)$$

as well as to the higher-order eccentricities of the overlap region in the transverse plane, defined as $\epsilon_n \equiv \epsilon_n e^{in\Phi_n} = -\langle r_\perp^n e^{in\phi} \rangle / \langle r_\perp^n \rangle$. In this case, the leading order expression for δd_\perp and eccentricity are $\delta d_\perp / d_\perp = \delta_d + \sum_{m=2}^4 p_{0;m} \beta_m$ and $\epsilon_n \approx \epsilon_{n;0} + \sum_{m=2}^4 \mathbf{p}_{n;m}(\Omega_1, \Omega_2) \beta_m$, respectively. The variances have the following more general form

$$\left\langle \left(\frac{\delta d_\perp}{d_\perp} \right)^2 \right\rangle \approx \langle \delta_d^2 \rangle + \sum_{m,m'} \langle p_{0;m} p_{0;m'} \rangle \beta_m \beta_{m'}, \quad \langle \epsilon_n^2 \rangle \approx \langle \epsilon_{n;0}^2 \rangle + \sum_{m,m'} \langle \mathbf{p}_{n;m} \mathbf{p}_{n;m'}^* \rangle \beta_m \beta_{m'}. \quad (10)$$

The off-diagonal coefficients $\langle p_{0;m} p_{0;m'} \rangle_{m \neq m'}$ and $\langle \mathbf{p}_{n;m} \mathbf{p}_{n;m'}^* \rangle_{m \neq m'}$ may not vanish especially in the non-central collisions. These mixing contributions have been observed in my previous study of $\langle \epsilon_n^2 \rangle$ [14], and are expected to influence all other cumulants discussed above. I leave this interesting topic to a future study.

For a more quantitative estimation, I consider the liquid-drop model where the nucleon density distribution has a sharp surface. I limit the discussion to head-on collisions with nearly maximum overlap, i.e. the two nuclei not only have zero impact parameter, but are also aligned $\Omega_1 = \Omega_2$ to ensure the overlap region contains all the nucleons $N_{\text{part}} = 2A$. In this case it is easy to show (see Ref. [15] and Appendix B)

$$\frac{\delta d_\perp}{d_\perp} = \sqrt{\frac{5}{16\pi}} \beta_2 \left(\cos \gamma D_{0,0}^2 + \frac{\sin \gamma}{\sqrt{2}} [D_{0,2}^2 + D_{0,-2}^2] \right), \quad \epsilon_2 = -\sqrt{\frac{15}{2\pi}} \beta_2 \left(\cos \gamma D_{2,0}^2 + \frac{\sin \gamma}{\sqrt{2}} [D_{2,2}^2 + D_{2,-2}^2] \right), \quad (11)$$

where the $D_{m,m'}^l(\Omega)$ is the Wigner matrix. From this, one obtain directly the probability density distributions of $\delta d_\perp / d_\perp$ shown in the bottom row of Fig. 1 (the distribution for the prolate case was previously derived in a different context [36]). From these, one can easily integrate to obtain the expression for cumulants of any order, e.g.:

$$\begin{aligned} \left\langle \left(\frac{\delta d_\perp}{d_\perp} \right)^2 \right\rangle &= \beta_2^2 \frac{5}{16\pi} \int \left(\sum_m \alpha_{2,m} D_{0,m}^2 \right)^2 \frac{d\Omega}{8\pi^2} = \frac{1}{16\pi} \beta_2^2, \quad \alpha_{2,0} \equiv \cos \gamma, \quad \alpha_{2,\pm 2} \equiv \frac{\sin \gamma}{\sqrt{2}}, \\ \left\langle \left(\frac{\delta d_\perp}{d_\perp} \right)^3 \right\rangle &= \beta_2^3 \left(\frac{5}{16\pi} \right)^{3/2} \int \left(\sum_m \alpha_{2,m} D_{0,m}^2 \right)^3 \frac{d\Omega}{8\pi^2} = \frac{\sqrt{5}}{224\pi^{3/2}} \cos(3\gamma) \beta_2^3 \\ \left\langle \epsilon_2^2 \frac{\delta d_\perp}{d_\perp} \right\rangle &= \beta_2^3 \frac{15}{2\pi} \sqrt{\frac{5}{16\pi}} \int \left(\sum_m \alpha_{2,m} D_{2,m}^2 \right) \left(\sum_m \alpha_{2,m} D_{2,m}^2 \right)^* \left(\sum_m \alpha_{2,m} D_{0,m}^2 \right) \frac{d\Omega}{8\pi^2} = -\frac{3\sqrt{5}}{28\pi^{3/2}} \cos(3\gamma) \beta_2^3. \end{aligned} \quad (12)$$

The results for several cumulants of interest are listed in the Table I¹. If one uses the transverse nucleon density $N_{\text{part}}/S_{\perp} = d_{\perp}^2$ as the estimator as done in Ref. [29], the n^{th} -order cumulant would be larger by 2^n . The values for appropriately normalized cumulants are also given to the lower-right side of the observable.

The skewness and kurtosis of d_{\perp} are conventionally normalized by the variance,

$$S_d = \frac{C_d\{3\}}{C_d\{2\}^{3/2}}, \quad K_d = \frac{C_d\{4\}}{C_d\{2\}^2}. \quad (13)$$

The four and six-order cumulants of ϵ_2 are defined by $\text{nc}_{2,\epsilon}\{4\} = (\langle \epsilon_2^4 \rangle - 2\langle \epsilon_2^2 \rangle^2) / \langle \epsilon_2^2 \rangle^2$ and $\text{nc}_{2,\epsilon}\{6\} = (\langle \epsilon_2^6 \rangle - 9\langle \epsilon_2^4 \rangle \langle \epsilon_2^2 \rangle + 12\langle \epsilon_2^2 \rangle^3) / (4\langle \epsilon_2^2 \rangle^3)$, respectively. The normalization of $\langle \epsilon_2^2 \delta d_{\perp} / d_{\perp} \rangle$ is defined in two different ways,

$$\rho_{\text{orig}}(\epsilon_2^2, \delta d_{\perp} / d_{\perp}) = \frac{\langle \epsilon_2^2 \delta d_{\perp} / d_{\perp} \rangle}{\sqrt{(\langle \epsilon_2^4 \rangle - \langle \epsilon_2^2 \rangle^2) \langle (d_{\perp} / d_{\perp})^2 \rangle}}, \quad \rho(\epsilon_2^2, \delta d_{\perp} / d_{\perp}) = \frac{\langle \epsilon_2^2 \delta d_{\perp} / d_{\perp} \rangle}{\langle \epsilon_2^2 \rangle \sqrt{\langle (d_{\perp} / d_{\perp})^2 \rangle}}. \quad (14)$$

The ρ_{orig} is the original definition known as the Pearson correlation coefficient [29, 37]. The term involving ϵ_2 in its denominator can be expressed as,

$$\langle \epsilon_2^4 \rangle - \langle \epsilon_2^2 \rangle^2 \equiv \langle \epsilon_2^2 \rangle^2 + c_{2,\epsilon}\{4\} = \langle \epsilon_0^4 \rangle - \langle \epsilon_0^2 \rangle^2 + 2\langle \epsilon_0^2 \rangle \langle \mathbf{p}_2 \mathbf{p}_2^* \rangle \beta_2^2 + (\langle \mathbf{p}_2^2 \mathbf{p}_2^{*2} \rangle - \langle \mathbf{p}_2 \mathbf{p}_2^* \rangle^2) \beta_2^4. \quad (15)$$

This expression unfortunately contains also an annoying β_2^2 term that mixes nucleon fluctuations with deformation, which becomes dominant in the mid-central and peripheral collisions. The second definition, ρ , preferred in this paper, avoid such analytical complication. But for completeness, the values for both are quoted in Table I.

The normalization of four-particle symmetric cumulants between ϵ_2 and δd_{\perp} is defined as

$$\text{nc}(\epsilon_2^2, (\delta d_{\perp} / d_{\perp})^2) = \frac{\langle \epsilon_2^2 (\delta d_{\perp} / d_{\perp})^2 \rangle - \langle \epsilon_2^2 \rangle \langle (\delta d_{\perp} / d_{\perp})^2 \rangle}{\langle \epsilon_2^2 \rangle \langle (\delta d_{\perp} / d_{\perp})^2 \rangle}. \quad (16)$$

This correlator should be measurable with a few hundred millions of events in large systems. Lastly I also calculated the three-particle mixed harmonics $\langle \epsilon_2^2 \epsilon_4^* \rangle$, the β_2^4 dependence arises because the ϵ_4 has a β_2^2 dependence [15]. Interestingly, in the presence of only quadrupole deformation, one has $\langle \epsilon_2^2 \epsilon_4^* \rangle = \langle \epsilon_4^2 \rangle = \frac{45}{14\pi^2} \beta_2^4$. To limit the scope of this paper, I shall skip the discussion of these two observables and the fourth- and higher-order cumulants of ϵ_2 .

The results in Table I are obtained with the assumption $\Omega_1 = \Omega_2$. In reality, the selection of UCC events naturally encompasses a wider range of rotation angles and also a finite range of N_{part} , therefore I also study a second case which requires zero impact parameter but independent orientation for the two nuclei. Since the contributions of the two nuclei are independent, the additive nature of the cumulants implies that the value of the n^{th} -order cumulant of intensive quantity is reduced by a factor of 2^{n-1} , i.e a factor two smaller for $C_d\{2\}$ and $\langle \epsilon_2^2 \rangle$, a factor of four smaller for $C_d\{3\}$, and a factor of eight smaller for $C_d\{4\}$ and $\langle \epsilon_2^4 \rangle - 2\langle \epsilon_2^2 \rangle^2$ etc. These values are provided in Tab. II. In realistic model study, Ω_1 and Ω_2 are expected to be only partially aligned and the results for these observables are expected to be in between those given in Tab. I and Tab. II.

A few remarks are in order. The skewness $\langle \epsilon_2^2 (\delta d_{\perp} / d_{\perp}) \rangle$ and $\langle (\delta d_{\perp} / d_{\perp})^3 \rangle$ show clear sensitivity to triaxiality in the form of a characteristic $\cos(3\gamma)$ dependence, but with opposite sign. Therefore, when the nuclear shape is varied from prolate to oblate, $\langle \epsilon_2^2 (\delta d_{\perp} / d_{\perp}) \rangle$ is expected to change from negative to positive, while $\langle (\delta d_{\perp} / d_{\perp})^3 \rangle$ is expected to change from positive to negative. In particular, the normalized skewness ρ and S_d , defined in Eqs. (14) and (13), have equal magnitudes, suggesting a comparable sensitivity to the triaxiality. Secondly, all two- and four-particle correlators have no explicit γ dependence, while the six-particle eccentricity cumulant contains a small $\cos(6\gamma)$ modulation. An interesting case is the normalized fourth-order cumulant of ϵ_2 , $\text{nc}_2\{4\} = \langle v_2^4 \rangle / \langle v_2^2 \rangle^2 - 2 = -2/7$. Assuming linear-response relation $v_2\{2k\} = k_2 \epsilon_2\{2k\}$ and a large β_2 , one expects a large four-particle cumulant signal $v_2\{4\}$, $v_2\{4\} / v_2\{2\} = \epsilon_2\{4\} / \epsilon_2\{2\} \equiv (-\text{nc}_2\{4\})^{1/4} = 0.73$. This naturally explains the much larger $v_2\{4\}$ value in $^{238}\text{U} + ^{238}\text{U}$ collisions than that in $^{197}\text{Au} + ^{197}\text{Au}$ collisions due to the large β_2 for ^{238}U nucleus [17].

¹ The expression for 5th- and 6th-order cumulants of d_{\perp} are $C_d\{5\} = -\frac{15\sqrt{5}}{9856\pi^{5/2}} \cos(3\gamma)\beta_2^5$ and $C_d\{6\} = \frac{15}{7007 \times 512\pi^3} (113 - 90 \cos(6\gamma))\beta_2^6$.

$\langle(\delta d_{\perp}/d_{\perp})^2\rangle$		$\langle(\delta d_{\perp}/d_{\perp})^3\rangle$		$\langle(\delta d_{\perp}/d_{\perp})^4\rangle - 3\langle(\delta d_{\perp}/d_{\perp})^2\rangle^2$	
$\frac{1}{16\pi}\beta_2^2$		$\frac{\sqrt{5}}{224\pi^{3/2}}\cos(3\gamma)\beta_2^3$	$\frac{2\sqrt{5}}{7}\cos(3\gamma)$	$-\frac{3}{896\pi^2}\beta_2^4$	$-6/7$
$\langle\varepsilon_2^2\rangle$		$\langle\varepsilon_2^4\rangle - 2\langle\varepsilon_2^2\rangle^2$		$(\langle\varepsilon_2^6\rangle - 9\langle\varepsilon_2^4\rangle\langle\varepsilon_2^2\rangle + 12\langle\varepsilon_2^2\rangle^3)/4$	
$\frac{3}{2\pi}\beta_2^2$		$-\frac{9}{7\pi^2}\beta_2^4$	$-4/7$	$\frac{27(373-25\cos(6\gamma))}{8008\pi^3}\beta_2^6$	$\frac{373-25\cos(6\gamma)}{1001}$
$\langle\varepsilon_2^2(\delta d_{\perp}/d_{\perp})\rangle$		$\langle\varepsilon_2^2(\delta d_{\perp}/d_{\perp})^2\rangle - \langle\varepsilon_2^2\rangle\langle(\delta d_{\perp}/d_{\perp})^2\rangle$		$\langle\varepsilon_2^2\varepsilon_4^*\rangle$	
$-\frac{3\sqrt{5}}{28\pi^{3/2}}\cos(3\gamma)\beta_2^3$	$-\frac{2\sqrt{5}}{7}\cos(3\gamma), -\sqrt{\frac{20}{21}}\cos(3\gamma)$	$-\frac{3}{112\pi^2}\beta_2^4$	$-1/4$	$\frac{45}{14\pi^2}\beta_2^4$	

TABLE I. The value of various cumulants of ε_2 and d_{\perp} , calculated for nucleus with sharp surface by setting $a = 0$ in Eq. (1). The two nuclei are placed with zero impact parameter and results are obtained by averaging over common random orientations. For many observables, I also provide the values after normalizing with second-order cumulants, which are listed in the bottom-right half of the cell (In the case of $\langle\varepsilon_2^2(\delta d_{\perp}/d_{\perp})\rangle$, both values of ρ (the first number) and ρ_{orig} (the second number) are provided).

$\langle(\delta d_{\perp}/d_{\perp})^2\rangle$		$\langle(\delta d_{\perp}/d_{\perp})^3\rangle$		$\langle(\delta d_{\perp}/d_{\perp})^4\rangle - 3\langle(\delta d_{\perp}/d_{\perp})^2\rangle^2$	
$\frac{1}{32\pi}\beta_2^2$		$\frac{\sqrt{5}}{896\pi^{3/2}}\cos(3\gamma)\beta_2^3$	$\frac{\sqrt{10}}{7}\cos(3\gamma)$	$-\frac{3}{7168\pi^2}\beta_2^4$	$-3/7$
$\langle\varepsilon_2^2\rangle$		$\langle\varepsilon_2^4\rangle - 2\langle\varepsilon_2^2\rangle^2$		$(\langle\varepsilon_2^6\rangle - 9\langle\varepsilon_2^4\rangle\langle\varepsilon_2^2\rangle + 12\langle\varepsilon_2^2\rangle^3)/4$	
$\frac{3}{4\pi}\beta_2^2$		$-\frac{9}{56\pi^2}\beta_2^4$	$-2/7$	$\frac{27(373-25\cos(6\gamma))}{32\times 8008\pi^3}\beta_2^6$	$\frac{373-25\cos(6\gamma)}{4004}$
$\langle\varepsilon_2^2(\delta d_{\perp}/d_{\perp})\rangle$		$\langle\varepsilon_2^2(\delta d_{\perp}/d_{\perp})^2\rangle - \langle\varepsilon_2^2\rangle\langle(\delta d_{\perp}/d_{\perp})^2\rangle$		$\langle\varepsilon_2^2\varepsilon_4^*\rangle$	
$-\frac{3\sqrt{5}}{112\pi^{3/2}}\cos(3\gamma)\beta_2^3$	$-\frac{\sqrt{10}}{7}\cos(3\gamma), -\sqrt{\frac{2}{7}}\cos(3\gamma)$	$-\frac{3}{896\pi^2}\beta_2^4$	$-1/8$	$\frac{45}{56\pi^2}\beta_2^4$	

TABLE II. Same calculation as Table I, except assuming independent random orientations for the two nuclei.

III. MODEL SETUP

For a more realistic estimation of influence of nuclear deformation, a Monte-Carlo Glauber model [38] is used to simulate collisions of ^{238}U and ^{96}Zr systems. These systems are chosen because the experimental collision data exist already. The setup of the model and the data used in this analysis are exactly the same as those used in my previous work [15]. The nucleons are assumed to have a hard-core of 0.4 fm in radii, with a density described by Eq. (1). The nuclear radius R_0 and the surface thickness a are chosen to be $R_0 = 6.81$ fm and $a = 0.55$ fm for ^{238}U and $R_0 = 5.09$ fm and $a = 0.52$ fm for ^{96}Zr , respectively. The nucleon-nucleon inelastic cross-section is chosen to be $\sigma_{\text{nn}} = 42$ mb at $\sqrt{s_{\text{NN}}} = 200$ GeV. In each collision event, nucleons are generated in each nucleus at a random impact parameter. Each nucleus is then rotated by randomly generated Euler angles before they are set on a straight line trajectory towards each other along the z direction. From this, the nucleons in the overlap region are identified, which are used to calculate the ε_2 and d_{\perp} defined in Eqs. (2) and (4), and the results are presented as a function of N_{part} . Most of the study focuses on the influence of quadrupole deformation, but I also performed a limited study on the influence of the observables from octupole and hexadecapole deformations, for which additional axial symmetric component are added to the nuclear surface (see Eq. (9)). A special study is performed to also investigate the presence of multiple shape components, where two or three nonzero values for β_2 , β_3 and β_4 are enabled.

It is well known that particle production in nucleus-nucleus collisions scale only approximately with N_{part} . A better scaling can be achieved by considering the constituent quarks as effective degrees-of-freedom for particle production [39–43], which would naturally give rise to slightly different ε_2 and d_{\perp} in each event. Defining centrality with constituent quarks is also expected to change the fluctuations of eccentricity, and provides a way to quantify the centrality smearing effects (also known as volume fluctuations) [44–46]. For this purpose, a quark Glauber model from Ref. [41] is used. Three quark constituents are generated for each nucleon according to the “mod” configuration [47], which ensures that the radial distribution of the three constituents after re-centering follows the proton form factor $\rho_{\text{proton}}(r) = e^{-r/r_0}$ with $r_0 = 0.234$ fm [48]. The value of quark-quark cross-section is chosen to be $\sigma_{\text{qq}} = 8.2$ mb in order to match the σ_{nn} . The ε_2 and d_{\perp} are then calculated from the list of quark participants in the overlap region,

and the number of quark participants N_{quark} is used as an alternative centrality estimator.

In the presence of large deformation, the total volume of the nucleus increases slightly. Considering the quadrupole deformation only, for the largest value considered, $\beta_2 = 0.34$, the ratio to the original volume is approximately (exact for sharp surface nucleus) $1 + \frac{3}{4\pi}\beta_2^2 + \frac{\sqrt{5}}{28\pi^{3/2}}\cos(3\gamma)\beta_2^3 = 1.021 + 0.0004\cos(3\gamma)$. To keep the overall volume fixed, it would require less than 1% decrease of the R_0 , which is safely ignored in the present study.

The results for each cumulant observable are obtained in four different ways. Taking the variance $\langle(\delta d_\perp/d_\perp)^2\rangle$ for instance, d_\perp in each event is calculated either from nucleons or quarks in the Glauber model, after which the averaging “ $\langle\rangle$ ” is then performed for events with the same N_{part} or the same N_{quark} . The latter can produce different variances due to slightly different volume fluctuations which can be quite important in the UCC region. Each cumulant can be obtained from either nucleons or quarks and then plotted as a function of N_{part} or N_{quark} .

I also carried out an independent study based on AMPT transport model to understand the conversion from ε_2 and d_\perp in the initial overlap to v_2 and $[p_T]$ in the final state. Unfortunately, this model is known to have the wrong hydrodynamic response for the radial flow [14, 49], therefore it is only used to study the parametric dependence of various observables on (β_2, γ) and compare with the trends in the initial state. The detail of the model and the study are presented in Appendix A.

IV. RESULTS

To highlight the general feature of the (β_2, γ) dependence, Fig. 2 shows the correlations between ε_2 and $\delta d_\perp/d_\perp = -\delta R_\perp/R_\perp$ calculated with nucleon Glauber model in the 0–0.1% most central U+U collisions selected on N_{part} . They can be contrasted directly with the expectations illustrated by Fig. 1. A clear anticorrelation (positive correlation) between ε_2 and $\delta d_\perp/d_\perp$ is observed for the prolate (oblate) deformation as expected. The distribution of $\delta d_\perp/d_\perp$ also indicates clearly a positive (negative) skewness as expected. These distributions are broader than the ideal case in Fig. 1 due to randomness of Ω_1 relative to Ω_2 , surface diffuseness, smearing from nucleon position fluctuations and centrality selection.

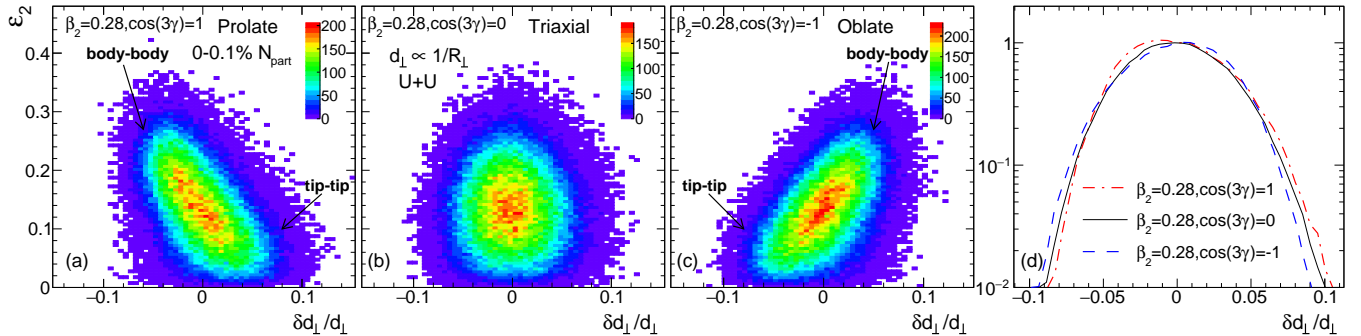


FIG. 2. Correlation between ε_2 and $\delta d_\perp/d_\perp$ for quadrupole deformation $\beta_2 = 0.28$ with prolate (left panel), rigid triaxial (second left panel) and oblate (third left panel) shape in the 0–0.1% most central U+U collisions selected on N_{part} . The right panel show the distributions of $\delta d_\perp/d_\perp$ in the three cases.

The goal of this paper is to explore the (β_2, γ) dependence of various cumulants in Tabs. I and II, and to provide guidance for the experimental measurements. The main finding is that the β_2, γ dependence for the n^{th} -order cumulant can be described by a simple equation with the following general form

$$a' + (b' + c' \cos(3\gamma))\beta_2^n, \quad (19)$$

including the variance $\langle(\delta d_\perp/d_\perp)^2\rangle$ and $\langle\varepsilon_2^2\rangle$, the skewness $\langle(\delta d_\perp/d_\perp)^3\rangle$ and $\langle\varepsilon_2^3\varepsilon_2/d_\perp\rangle$, and the kurtosis $\langle(\delta d_\perp/d_\perp)^4\rangle - 3\langle(\delta d_\perp/d_\perp)^2\rangle^2$ and $\langle\varepsilon_2^4\rangle - 2\langle\varepsilon_2^2\rangle^2$. It is remarkable that most γ dependences can be described by a $\cos(3\gamma)$ function, and the higher-order terms allowed by symmetry $\cos(6\gamma)$, $\cos(9\gamma)$ etc are very small. The coefficients a' , b' and c' are functions of centrality and collision systems, but are independent of β_2 and γ . The coefficient a' represents the values

² In principle full expression should also contain contribution from volume fluctuations, i.e. $\delta d_\perp/d_\perp = -\delta R_\perp/R_\perp + \frac{1}{2}\delta N_{\text{part}}/N_{\text{part}}$. However, the second term drops out when one classifies events according to N_{part} .

for spherical nuclei, it is usually a strong function of centrality and size of the collision systems. In contrast, the values of b' and c' are similar between nucleon and quark Glauber models and between U+U vs Zr+Zr (i.e. independent of collision systems). They also have rather weak dependence on event centrality. These behavior are the result of geometrical effects: the deformation changes the distribution of nucleons in the entire nucleus, therefore the values of b' and c' in each collision event depend only on the Euler angles of the two nuclei and the impact parameter, and they should be insensitive to the size of the collision system in the Glauber model.

The results are organized as follows. Section IV A discusses the variance of d_\perp in detail, which corresponds to experimentally measured $[p_T]$ variance. Results of higher-order cumulants, skewness and kurtosis of d_\perp fluctuations, are presented in Sec. IV B. Section IV C considers the mixed cumulant between d_\perp and ε_2 , which is identified to be the most promising observable to constrain γ . I then summarize in Sec. IV D the Glauber results in terms of Eq. (17) and discuss the effects of volume fluctuations, and the centrality and system dependences of the results. The results of the AMPT model are included in the Appendix A.

A. Variance of d_\perp fluctuations

In the hydrodynamic picture, the variance of d_\perp fluctuation is proportional to the variance of $[p_T]$ fluctuation, $C_d\{2\} = \langle (\delta d_\perp / d_\perp)^2 \rangle \propto \langle (\delta [p_T] / \langle p_T \rangle)^2 \rangle$.

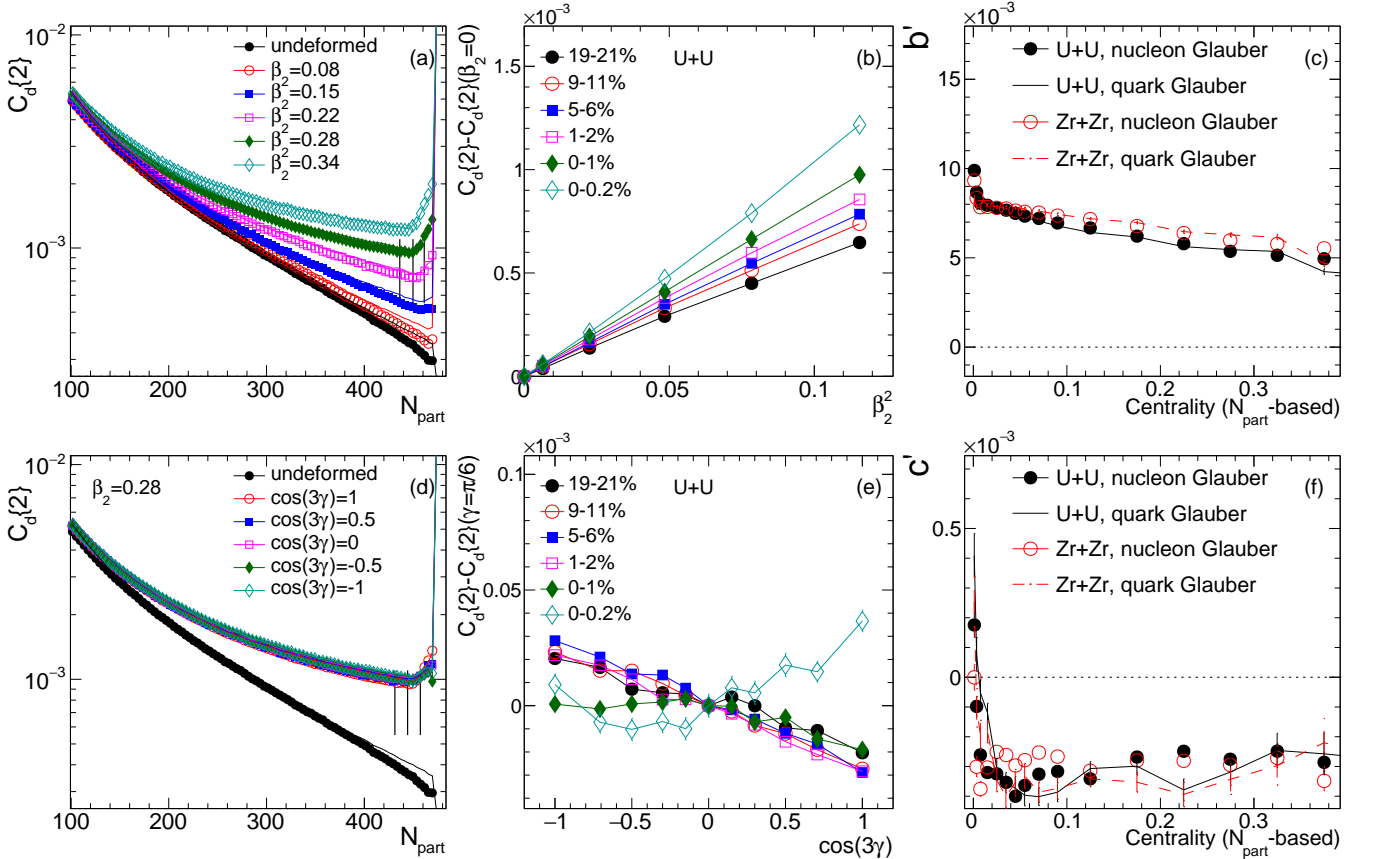


FIG. 3. $\langle (\delta d_\perp / d_\perp)^2 \rangle$ for several β_2 values with $\gamma = 0$ (top row) and several γ values with $\beta_2 = 0.28$ (bottom row) in U+U collisions. The left column show the N_{part} dependence where markers and lines represent d_\perp obtained with nucleons and quarks, respectively. The middle column shows results in several centrality ranges, which follows a linear function of β_2^2 (top panel) or $\cos(3\gamma)$ (bottom panel). The right column shows the coefficients b' (top) and c' (bottom) as a function of centrality in U+U (black) and Zr+Zr (red) systems for d_\perp calculated from nucleons (markers) or quarks (lines). The three vertical lines in the left column mark the locations of 2%, 1% and 0.2% centrality, respectively.

The left column of Fig. 3 shows the N_{part} dependence of $C_d\{2\}$ for various values of β_2 or γ with fixed $\beta_2 = 0.28$ in U+U collisions, calculated from the participating nucleons. In the absence of deformation, the $C_d\{2\}$ decreases approximately as a power-law function of N_{part} . The presence of large β_2 increases $C_d\{2\}$ over a very broad centrality range. On the other hand, the triaxiality parameter γ only has a small influence, as reflected by the clustering of all

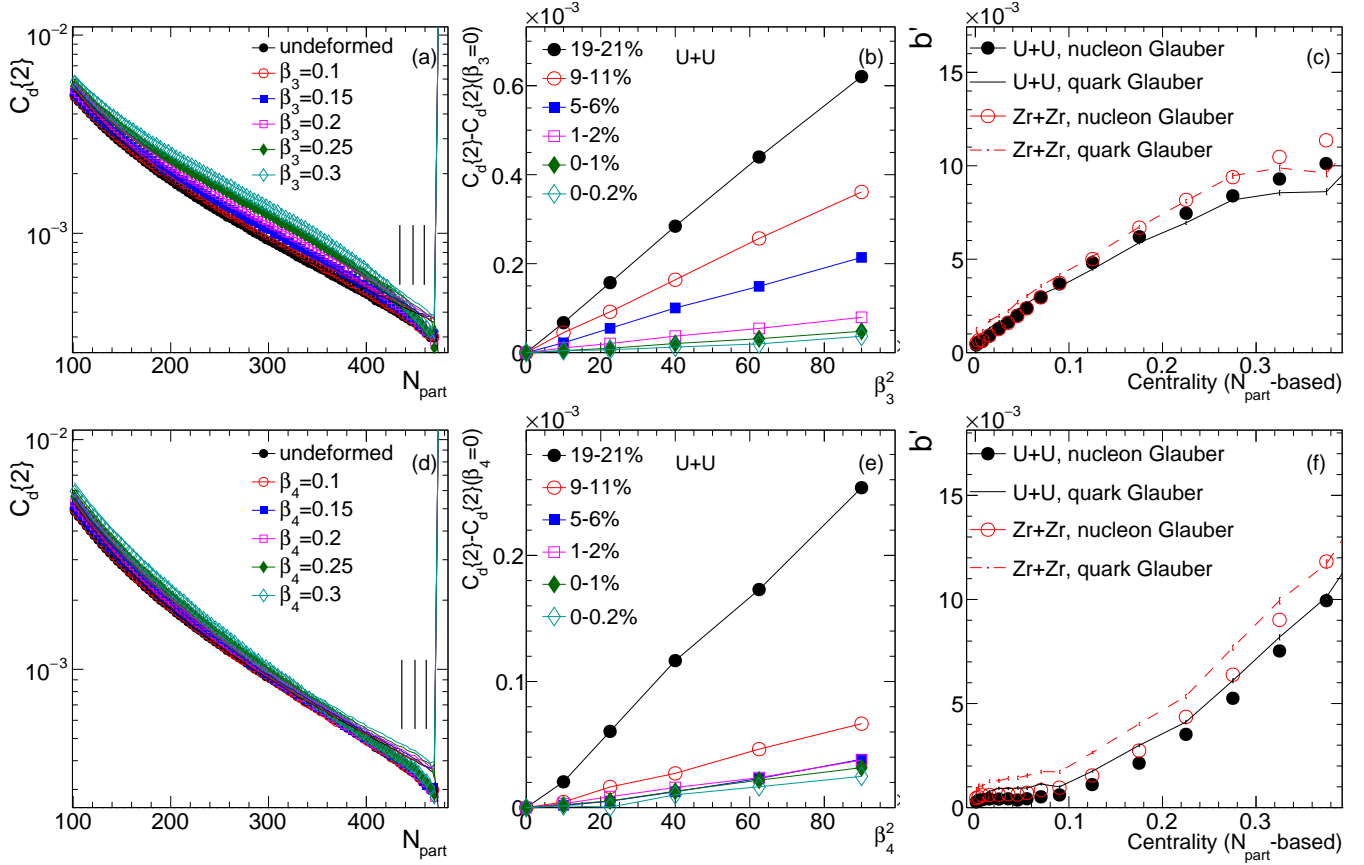


FIG. 4. $\langle(\delta d_{\perp}/d_{\perp})^2\rangle$ for several values of β_3 (top row) and β_4 (bottom row) as a function of N_{part} (left column) or β_n^2 (middle column) in U+U collisions. The latter dependences can be described by a simple $a' + b'\beta_n^2$ function. The right column summarizes the values of b' from the middle column as a function of centrality in U+U (black) and Zr+Zr (red) systems.

different curves in the bottom-left panel. In the same panels, I also show results calculated from quark participants as solid lines, with the same color as those calculated from nucleon participants. Little differences are observed between the two, implying that the influences of deformation are insensitive to nucleon substructures.

To quantify the (β_2, γ) dependencies, $C_d\{2\}$ values obtained for fixed N_{part} are averaged in narrow centrality ranges, which are then plotted as a function of β_2^2 or $\cos(3\gamma)$ in the middle column of Fig. 3. Very good linear trends are observed in most of the cases, confirming Eq. (17)³. The slopes in the middle-top panel equal to $b' + c'$ (since $\gamma = 0$) and the slopes in the middle-bottom panel equal to $c'\beta_2^2$. The two panels in the right column summarize the centrality dependence of b' and c' , respectively. They are shown for d_{\perp} calculated from both nucleons and quarks in U+U and Zr+Zr collisions. It is quite remarkable that the values of b' and c' are insensitive to subnucleon structures and are similar in both collision systems, this is expected since deformation influences the global geometry of the overlap region. The values of c' is about a factor 20–30 smaller than b' . A qualitatively similar functional form was also observed between $\langle\varepsilon_2^2\rangle$ and (β_2, γ) in a previous study [15].

Although the axial quadrupole distortion is the nuclear deformation of primary importance, contributions from octupole and hexadecapole components often coexist and can be important in some regions of nuclear chart [50]. Therefore, it is interesting to study how d_{\perp} is affected by β_3 and β_4 . I have performed such calculations and the results are shown in Fig. 4 with a similar layout as Fig. 3. These higher-order deformations have no influence on the variance of d_{\perp} in the UCC region, but significant enhancement associated with β_3 is observed in near-central and mid-central collisions, and the β_4 only has a modest enhancement in the peripheral region. These enhancements can be described by a quadratic function $b'\beta_3^2$ or $b'\beta_4^2$ according to Eq. (10). The coefficients b' are shown in the right panels.

To better visualize and quantify the effects of deformation, Fig. 5 shows the ratios of $C_d\{2\}$ in U+U (top row) or in Zr+Zr (bottom) collisions. The results in the top row are obtained directly from the data from the left columns of

³ In 0–0.2% centrality one also observes significant $\cos(6\gamma)$ component in Fig. 3, but not in quark Glauber model.

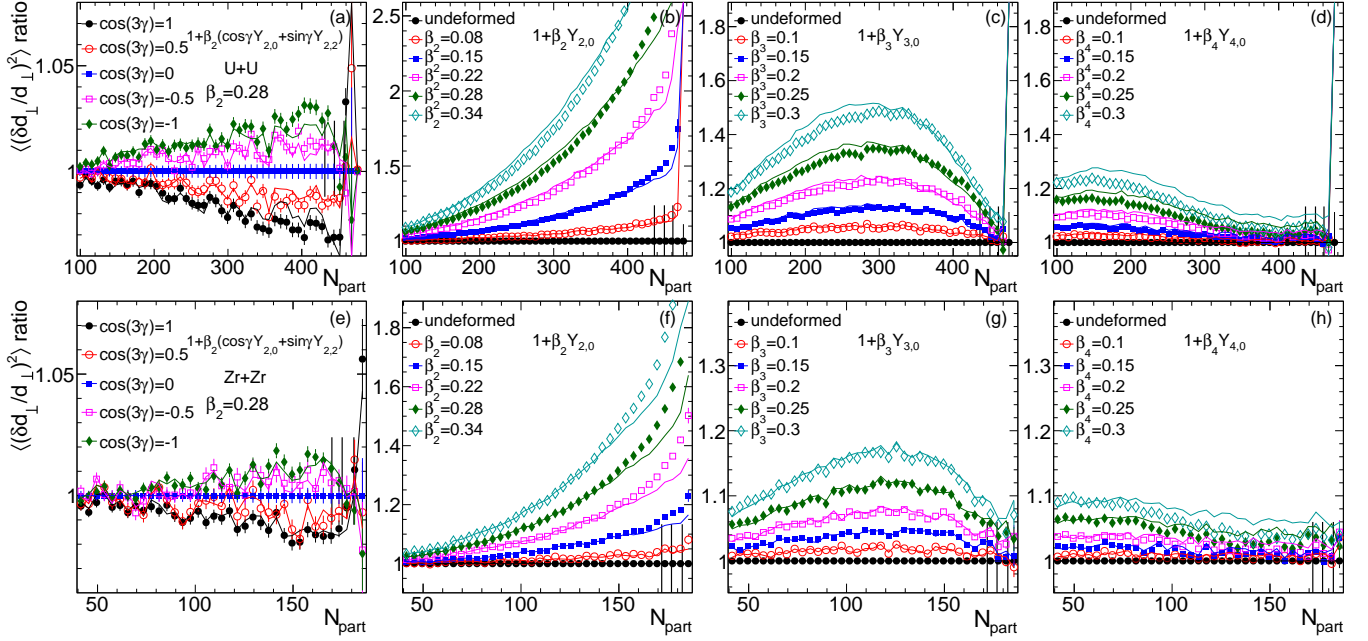


FIG. 5. Ratios of $\langle(\delta d_{\perp}/d_{\perp})^2\rangle$ to the default as a function of N_{part} for several values of $\cos(3\gamma)$ with $\beta_2 = 0.28$ (left column), several values of β_2 with $\cos(3\gamma) = 1$ (second column), several values of β_3 (third column) and β_4 (right column) in the U+U (top row) and the Zr+Zr (bottom row) collisions. The results calculated using nucleons or quarks are shown in markers and lines respectively. The three vertical bars around unity mark the locations of 2%, 1% and 0.2% centrality, respectively.

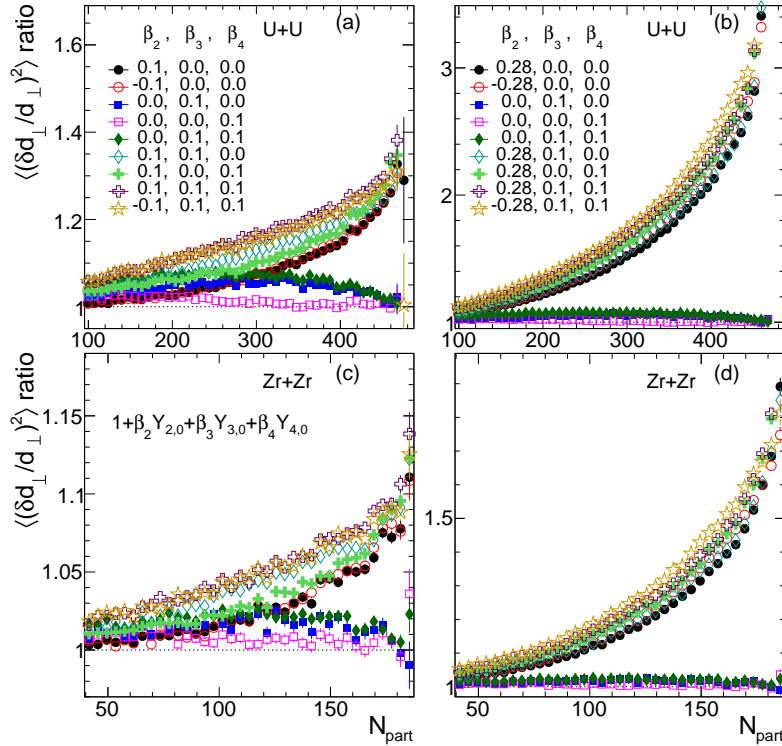


FIG. 6. Ratio of $\langle(\delta d_{\perp}/d_{\perp})^2\rangle$ for U+U (top row) and Zr+Zr (bottom row) collisions, relative to spherical case, as a function of N_{part} for different combinations of β_2, β_3 and β_4 as indicated in the top panels. The left column shows results with small $\beta_2 = 0.1$, while the right column shows results with large $\beta_2 = 0.28$. Both d_{\perp} and centrality are based on nucleon participants.

Figs. 3 and 4. These results can be related to the ratios of $\langle(\delta[p_T]/\langle p_T \rangle)^2\rangle$ between two systems with similar mass number but different deformation parameters. Most trends are obvious, but the results for different γ cases deserve some discussion. The separation between different γ cases increases linearly with N_{part} , reaching its maximum around 2% centrality and then decreasing in the more central region. The maximum relative difference is about 3–4%, which is about twice of the influence of γ for ε_2 [15]. As discussed later, such a γ dependence may arise from the higher-order expansion of $\delta d_\perp/d_\perp$ in powers of β_2 , which is particularly important for the kurtosis of the d_\perp fluctuations.

It is also interesting to study how the fluctuations of d_\perp depend on the simultaneous presence of quadrupole and higher-order deformations, in particular, whether the contribution from each component to d_\perp is independent of each other. For this exploratory study, only combinations of axial-symmetric components $Y_{n,0}$, $n = 2, 3, 4$ are considered. The analysis is carried out for different combinations of $(\beta_2, \beta_3, \beta_4)$ from the values $\beta_2 = \pm 0.1, 0$, $\beta_3 = 0.1, 0$, and $\beta_4 = 0.1, 0$, and results are shown in the left column of Fig. 6. The contributions from different deformation components are not fully independent of each other. In particular, the influence of β_4 and to some extent also β_3 is enhanced in the presence of β_2 . This suggests that the mixing between different deformation, i.e. terms such as $\beta_2\beta_4$, $\beta_2\beta_3$ and $\beta_3\beta_4$ in Eq. (10) are more important, but these nonlinear effects are always very small in the UCC region. The right column of Fig. 6 considers a different scenario where the quadrupole component $\beta_2 = 0.28$ is much larger than the octupole and hexadecapole. Similar conclusions can be drawn.

B. Skewness and kurtosis of d_\perp fluctuations

Figure 7 shows the results of skewness $C_d\{3\} = \langle(\delta d_\perp/d_\perp)^3\rangle$, which is directly related to the skewness of transverse momentum fluctuations $\langle(\delta[p_T]/\langle p_T \rangle)^3\rangle$, for different values of β_2 and γ with similar layout as Fig. 3. The N_{part} dependence in the left column show a strong sensitivity to the deformation parameter values across a broad centrality range. In particular, the $C_d\{3\}$ in the presence of large β_2 is nearly constant from the mid-central to central collisions, a salient feature observed in the skewness of $[p_T]$ fluctuations in the U+U data by the STAR collaboration [21]. The bottom panel also shows that the $C_d\{3\}$ is largest for prolate deformation $\cos(3\gamma) = 1$ and smallest for the oblate deformation $\cos(3\gamma) = -1$. In the latter case, $C_d\{3\}$ changes sign to negative in central collisions. The $C_d\{3\}$ values are plotted as a function of β_2^2 or $\cos(3\gamma)$ in the middle panels. Very good linear dependencies, described by Eq. (17), are observed.

The right panels show the centrality dependence of the coefficients b' and c' for various cases. The results are similar between U+U and Zr+Zr collisions, but the values of b' obtained from quark Glauber model are systematically larger, especially towards more peripheral collisions. The values of c' are larger than b' in the 0%–10% most central collisions, and are smaller than b' in the mid-central and peripheral collisions. This should be contrasted to the expectation of liquid-drop model, which predicts $b' = 0$ in the UCC region. The strong sensitivity to γ suggests that the skewness of the $[p_T]$ fluctuation is an excellent probe of nuclear triaxiality. For smaller Zr+Zr collision system, one does not observe a sign change from prolate deformation to oblate deformation even with $\beta_2 = 0.28$ (see Fig. 19 in Supplemental Material)

Results for kurtosis $C_d\{4\} = \langle(\delta d_\perp/d_\perp)^4\rangle - 3\langle(\delta d_\perp/d_\perp)^2\rangle^2$ are shown Fig. 8, which can be used to provide guidance on the behavior of kurtosis of transverse momentum fluctuations $\langle(\delta[p_T]/\langle p_T \rangle)^4\rangle - 3\langle(\delta[p_T]/\langle p_T \rangle)^2\rangle^2$. For large prolate deformation (top row), $C_d\{4\}$ changes sign in the UCC region. It also shows a strong dependence on γ (bottom row), i.e. $C_d\{4\}$ becomes more negative when nuclear shape change from prolate to oblate. These dependencies again can be parametrized according to Eq. (17). The centrality dependence of the extracted coefficients b' and c' are shown in the right panels. Besides the similarity between U+U and Zr+Zr, one finds $b' \approx -c'$ in the case of nucleon Glauber model, but $|b'| \gg |c'|$ in the quark Glauber model. The origin for this is related to a small $\cos(3\gamma)$ dependence in the $C_d\{2\}$, which will be discussed later.

The behavior of the high-order cumulants are often analyzed in terms of cumulant ratios. In an independent source picture and without deformation, the cumulants of intensive quantities scales approximately as $C_d\{k\} \sim 1/N_{\text{part}}^{k-1}$. The normalized skewness S_d and normalized kurtosis K_d in Eq. (13) are expected to scale naively as $S_d \sim 1/\sqrt{N_{\text{part}}}$ and $K_d \sim 1/N_{\text{part}}$, respectively. The results of Glauber model using N_{part} -based event averaging in Fig. 7 show clear deviation from this scaling expectation, although results obtained using N_{quark} -based event averaging are closer to this scaling. The presence of nuclear deformation is expected to cause further deviation from this baseline. The top row of Fig. 9 shows the S_d (left two panels) and K_d (right two panels) as a function of N_{part} for various β_2 and γ values. In the presence of large β_2 , the values of S_d are greatly enhanced, while the values of K_d decrease more strongly and even change sign in the UCC region. As one varies γ from prolate to oblate with fixed $\beta_2 = 0.28$, the behavior of S_d changes from an increase with N_{part} to a decrease with N_{part} , while K_d decreases nearly linearly with N_{part} with an increasingly larger slope. The results of K_d suggest a fairly sizable $\cos(3\gamma)$ component on the order of 0.1–0.2. As mentioned earlier, the origin is related to the residual $\cos(3\gamma)$ dependence in the $C_d\{2\}$ in Fig. 5. This

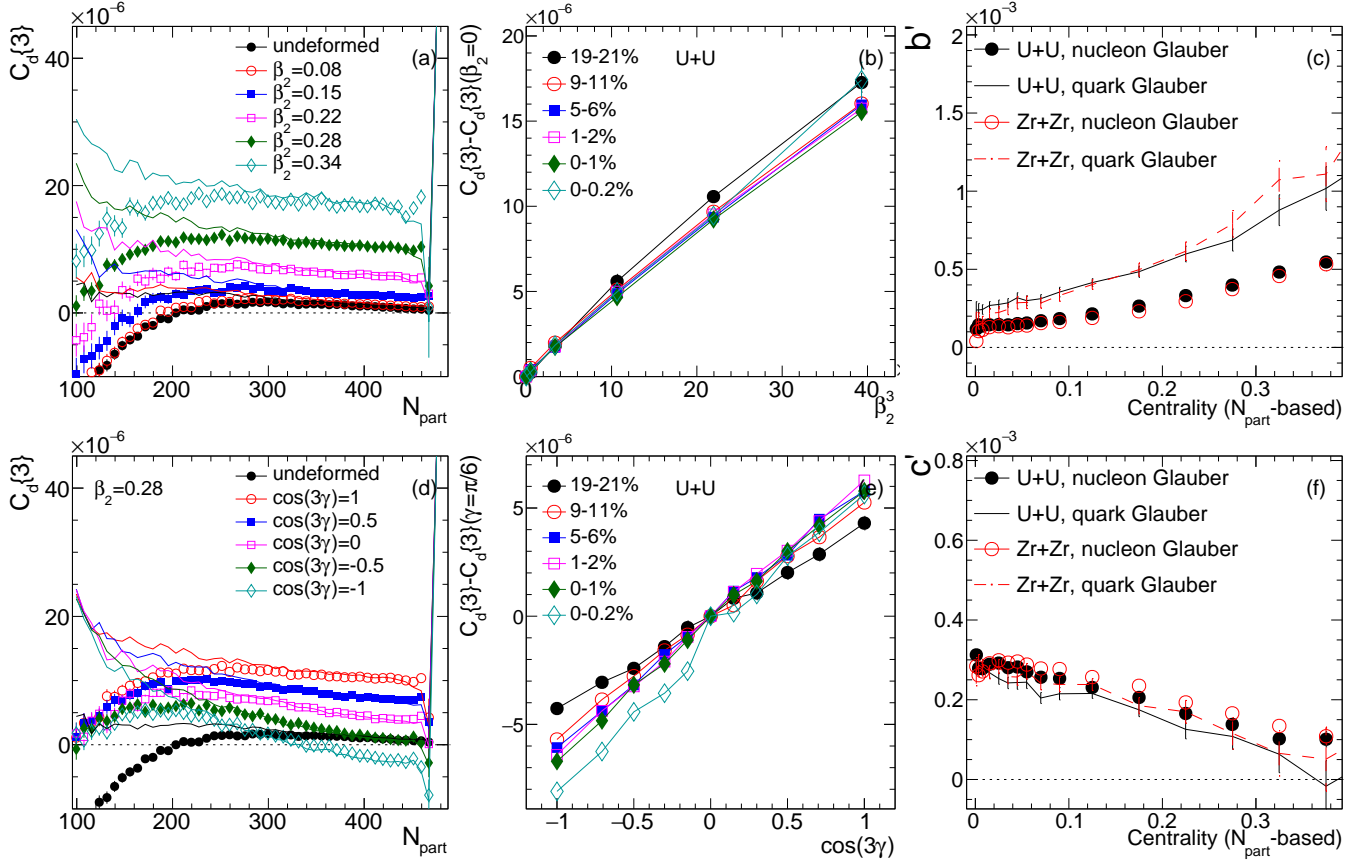


FIG. 7. The skewness $\langle (\delta d_1/d_1)^3 \rangle$ for several β_2 values with $\gamma = 0$ (top row) and several γ values with $\beta_2 = 0.28$ (bottom row). The left column shows the N_{part} dependence where markers and lines correspond d_1 obtained with nucleons and quarks, respectively. The middle column shows the respective results in several centrality ranges based on N_{part} , which can be mostly described by a linear function of β_2^3 (top panel) or $\cos(3\gamma)$ (bottom panel) via Eq. (17). The right column summarizes extracted coefficients b' (top) and c' (bottom) as a function of centrality in U+U (black) and Zr+Zr (red) systems calculated from nucleons (markers) or quarks (lines).

small γ dependence at the level of $\Delta C_d\{2\}/C_d\{2\} \approx \pm 0.03$ is found to contribute to the kurtosis approximately as $\Delta K_d = \frac{\Delta C_d\{4\}}{C_d\{2\}^2} - 6 \frac{\Delta C_d\{2\}}{C_d\{2\}} \approx -4 \frac{\Delta C_d\{2\}}{C_d\{2\}} \approx \mp 0.12$.

The normalized skewness S_d and kurtosis K_d , while easier to construct experimentally, mix up the contributions from nucleon fluctuations and nuclear deformation, which preclude a direct and intuitive interpretation of the results. Therefore, I propose a modified form of the normalized cumulants,

$$S_{d,\text{sub}} \equiv \frac{C_d\{3\} - C_d\{3\}|_{\beta_2=0}}{(C_d\{2\} - C_d\{2\}|_{\beta_2=0})^{3/2}} \equiv S_d(\beta_2 = \infty), \quad K_{d,\text{sub}} \equiv \frac{C_d\{4\} - C_d\{4\}|_{\beta_2=0}}{(C_d\{2\} - C_d\{2\}|_{\beta_2=0})^2} \equiv K_d(\beta_2 = \infty) \quad (18)$$

With this definition, the baseline contributions are subtracted in the numerator and denominator and the β_2 dependence is expected to cancel. The final results contain only the $\cos(3\gamma)$ dependence and can be compared directly with the normalized quantities in Tables I and II. Another important point is that the values of the normalized cumulant are expected to lie in between two limits

$$S_d(\beta_2 = 0) < S_d(\beta_2) < S_{d,\text{sub}}, \quad K_{d,\text{sub}} < K_d(\beta_2) < K_d(\beta_2 = 0). \quad (19)$$

The bottom panels of Fig. 9 show the results for these modified quantities. Results for different β_2 values, as shown by the first panel for $S_{d,\text{sub}}$ and the third panel for $K_{d,\text{sub}}$, nearly collapse on a common curve, confirming the earlier statement that these observables are a great way to isolate the coefficient b' and c' in Eq (17). The same panels also show the range of the predicted values from Tabs. I and II by the shaded gray boxes. Remarkably, the values predicted from the full Monte Carlo Glauber model falls within the ranges from the simple analytical estimates. These results

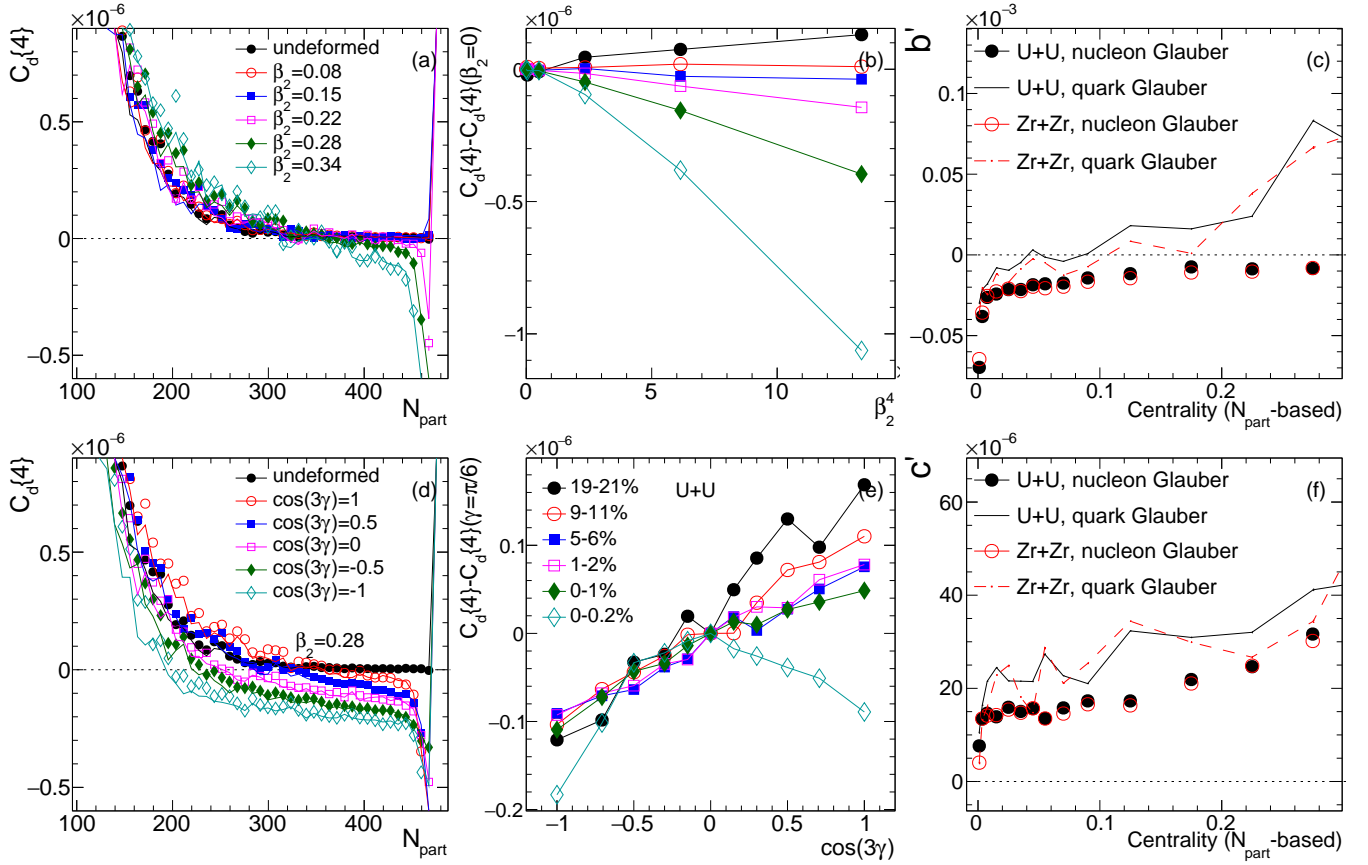


FIG. 8. The kurtosis of $p(d_{\perp})$ for several β_2 values with $\gamma = 0$ (top row) and several γ values with $\beta_2 = 0.28$ (bottom row). The left column shows the N_{part} dependence where markers and lines correspond to d_{\perp} obtained with nucleons and quarks, respectively. The middle column shows the respective results in several centrality ranges based on N_{part} , which can be mostly described by a linear function of β_2^4 (top panel) or $\cos(3\gamma)$ (bottom panel). The right column shows centrality dependence of extracted b' (top) and c' (bottom) via Eq. (17) in U+U (black) and Zr+Zr (red) systems for d_{\perp} calculated from nucleons (markers) or quarks (lines).

suggest an approximate parametrization $S_{d,\text{sub}} = b_0 + c_0 \cos 3\gamma$, with coefficient c_0 nearly independent of centrality and coefficient b_0 increasing from central to peripheral collisions.

Even though $S_{d,\text{sub}}$ and $K_{d,\text{sub}}$ can not be directly measured, they can be estimated by comparing results from collisions of two species A and B with similar mass numbers. Taking the skewness for example, one could construct the following ratio using Eq. (17),

$$S_{d,AB} = \frac{C_d\{3\}_A - C_d\{3\}_B}{(C_d\{2\}_A - C_d\{2\}_B)^{3/2}} \approx S_{d,\text{sub},A} \left(1 + \frac{3}{2}x^2 - \frac{b' + c' \cos(3\gamma_B)}{b' + c' \cos(3\gamma_A)}x^3 + \frac{15}{8}x^4 \right), \quad (20)$$

where $x = \beta_{2B}/\beta_{2A} \ll 1$ is assumed and I have ignored the negligible $\cos(3\gamma)$ term in $C_d\{2\}$. The b' and c' refers those of $C_d\{3\}$, which are expected to be the same for the two species. The ideal case for Eq. (20) is between a pair of isobaric system with different amount of deformations such as $^{96}\text{Zr}+^{96}\text{Zr}$ and $^{96}\text{Ru}+^{96}\text{Ru}$ collisions [51].

C. Correlation between eccentricity and d_{\perp}

Let us turn our attention to the skewness $\langle \varepsilon_2^2(\delta d_{\perp}/d_{\perp}) \rangle$ and the related final-state observable $\langle v_2^2(\delta[p_T]/[p_T]) \rangle$. This observable has been studied both experimentally [21, 52] and in models [14, 35], and, as discussed below, it has great potential in constraining the triaxiality of the colliding nuclei.

Figure 10 shows the results of $\langle \varepsilon_2^2(\delta d_{\perp}/d_{\perp}) \rangle$ for different values of β_2 and γ with the usual layout. The N_{part} dependences show a clear hierarchy between different β_2 and/or γ values, and the sensitivity to these parameters are

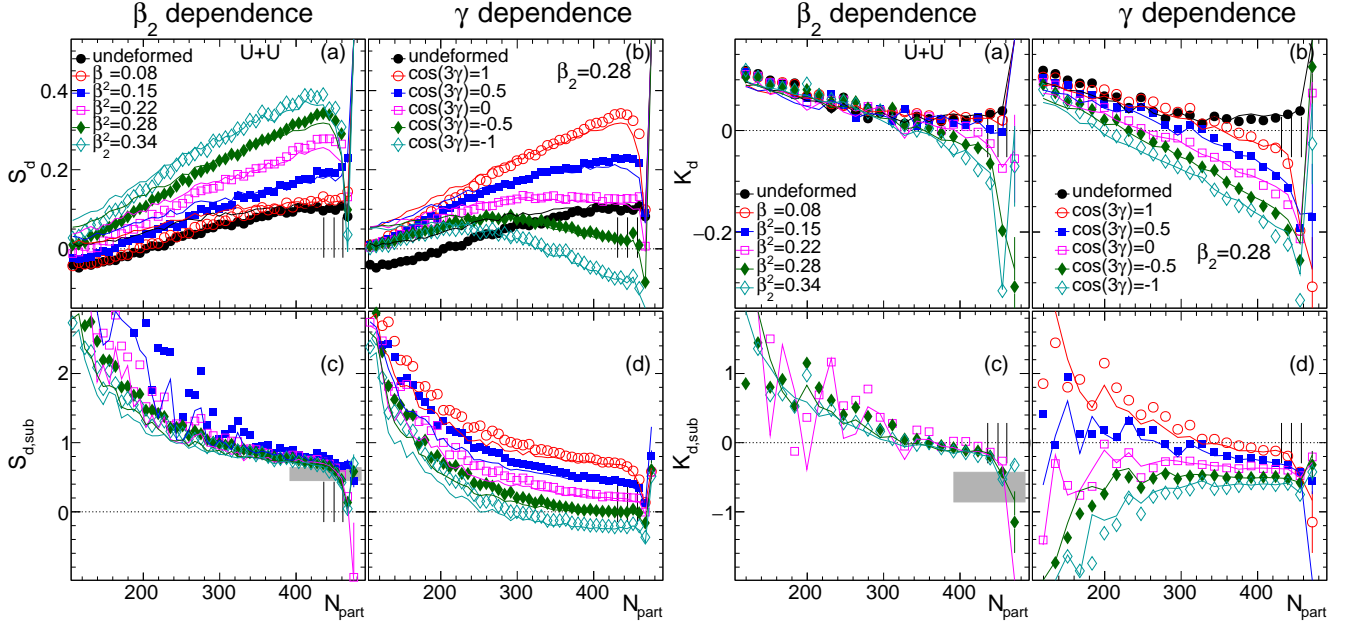


FIG. 9. Left part: N_{part} dependence of normalized skewness $S_d = C_d\{3\}/C_d\{2\}^{3/2}$ (top) and modified version $S_{d,\text{sub}}$ (bottom) for several β_2 values with $\gamma = 0$ (left) and for several γ values with $\beta_2 = 0.28$ (right) in U+U collisions. Right part: results for normalized kurtosis $K_d = C_d\{4\}/C_d\{2\}^2$ and $K_{d,\text{sub}}$ with the same layout. The shaded bands indicate the predicted range from Tabs. I and II.

clearly visible across a broad centrality range. In the absence of deformation, $\langle \varepsilon_2^2(\delta d_\perp/d_\perp) \rangle$ decreases gradually from peripheral to more central collisions but remains positive. For prolate deformation, as β_2 is increased, $\langle \varepsilon_2^2(\delta d_\perp/d_\perp) \rangle$ decreases over the entire centrality range, and becomes negative in the central region. However, for large oblate deformation, $\langle \varepsilon_2^2(\delta d_\perp/d_\perp) \rangle$ increases in the central region. This behavior is fully consistent with the expectation from Fig. 1.

The middle column shows the values of $\langle \varepsilon_2^2(\delta d_\perp/d_\perp) \rangle$ as a function of either β_2^3 or $\cos(3\gamma)$ in several narrow centrality ranges. A linear dependence is observed, consistent with the now familiar parametrization Eq. (17). The right panels show the centrality dependencies of b' and c' for various cases. The results are similar between U+U and Zr+Zr collisions and between nucleon Glauber and quark Glauber models. Both b' and c' are negative over the full centrality range. But the magnitude of c' is much larger than b' in the 0%–10% central collisions, and is smaller than b' in the mid-central and peripheral collisions. The sensitivity of $\langle \varepsilon_2^2(\delta d_\perp/d_\perp) \rangle$ to γ is stronger than $\langle (\delta d_\perp/d_\perp)^3 \rangle$, even though they are clearly complementary ⁴

The behavior of $\langle \varepsilon_2^2(\delta d_\perp/d_\perp) \rangle$ can be analyzed using the normalized quantity, $\rho_{\text{orig}}(\varepsilon_2^2, \delta d_\perp/d_\perp)$ and $\rho(\varepsilon_2^2, \delta d_\perp/d_\perp)$ defined in Eq. (14). They are directly related to the analog experimentally-accessible observable $\rho_{\text{orig}}(v_2^2, \delta[p_T]/[p_T])$ [37] and $\rho(v_2^2, \delta[p_T]/[p_T])$. The results of $\rho(\varepsilon_2^2, \delta d_\perp/d_\perp)$ are shown in the left part of Fig. 11. The second column shows an approximately linear function of β_2 for moderate value of β_2 , but nonlinear behavior shows up at small and larger β_2 . The reason for this complex β_2 dependence can be attributed to the a' terms in the numerator and the denominator. Following the example for the $S_{d,\text{sub}}$, I define a modified correlator by subtracting out the baseline effects,

$$\rho_{\text{sub}}(\varepsilon_2^2, \frac{\delta d_\perp}{d_\perp}) = \frac{\langle \varepsilon_2^2 \frac{\delta d_\perp}{d_\perp} \rangle - \langle \varepsilon_2^2 \frac{\delta d_\perp}{d_\perp} \rangle_{|\beta_2=0}}{(\langle \varepsilon_2^2 \rangle - \langle \varepsilon_2^2 \rangle_{|\beta_2=0}) \sqrt{\langle (\frac{\delta d_\perp}{d_\perp})^2 \rangle - \langle (\frac{\delta d_\perp}{d_\perp})^2 \rangle_{|\beta_2=0}}} \equiv \rho(\varepsilon_2^2, \frac{\delta d_\perp}{d_\perp})_{|\beta_2=\infty}, \quad (21)$$

Just like the case for skewness of the d_\perp fluctuations, the β_2 dependence completely cancels, and ρ_{sub} contains only the $\cos(3\gamma)$ dependence. Therefore it can be compared directly to the values in Tabs. I and II. The ρ in general is expected to be in between the value without deformation $\rho_{|\beta_2=0}$ and ρ_{sub} .

⁴ Given the importance of this observable, I also investigated the influence of β_3 and β_4 (see Fig. 22 in Appendix C). The influence is negligible in the UCC region. But one finds that β_3 enhances the value of $\langle \varepsilon_2^2(\delta d_\perp/d_\perp) \rangle$ in central collisions. In the peripheral region, both β_3 and β_4 reduce the signal, the relative change is less than 30% as long as $\beta_3, \beta_4 < 0.2$.

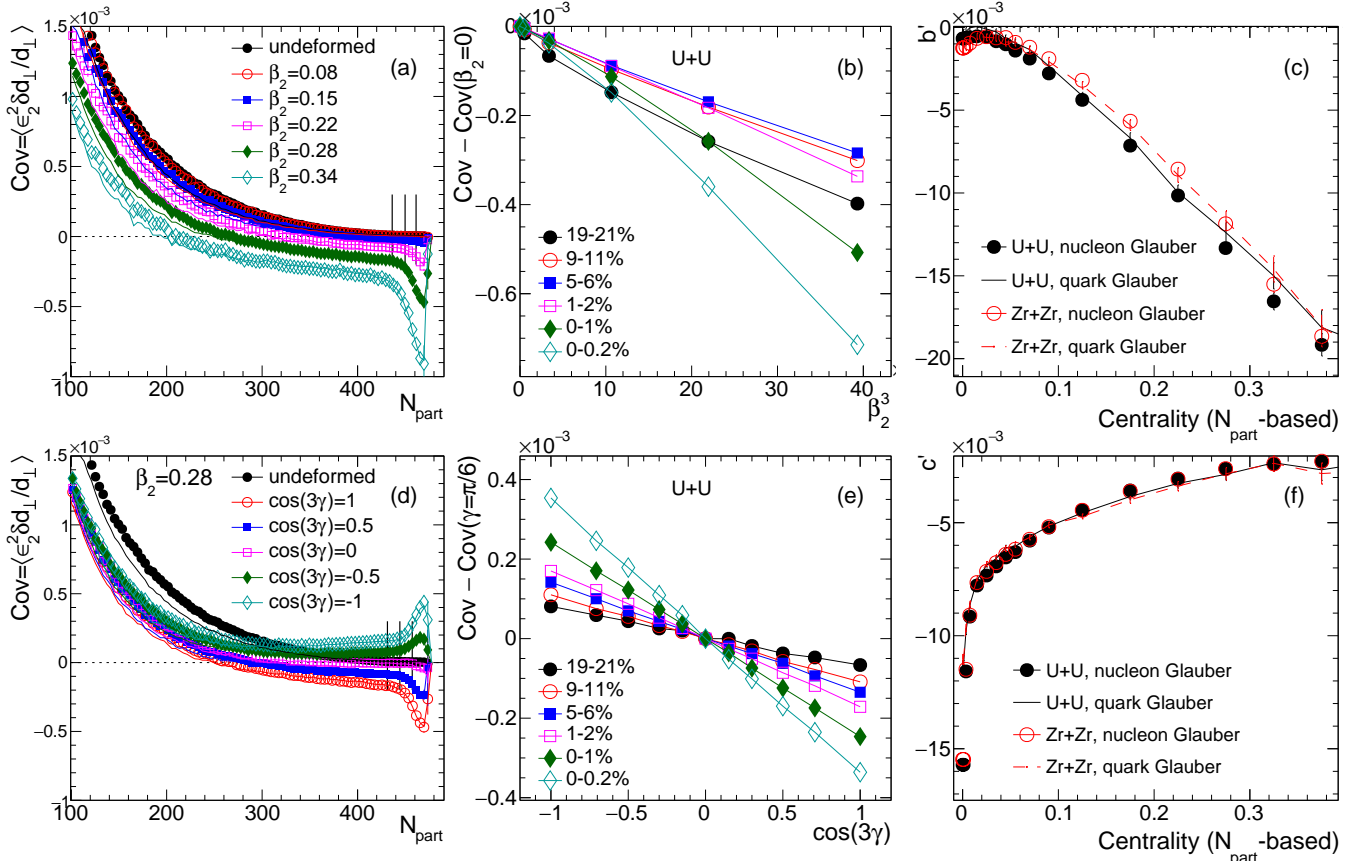


FIG. 10. The $\langle \varepsilon_2^2 \delta d_\perp / d_\perp \rangle$ for several β_2 values with $\gamma = 0$ (top row) and several γ values with $\beta_2 = 0.28$ (bottom row). The left column shows the N_{part} dependence. The middle column shows the respective results in several centrality ranges based on N_{part} . The right column summarizes the centrality dependence of b' (top) and c' (bottom) obtained via Eq. (17) in U+U (black) and Zr+Zr (red) collisions for ε_2 and d_\perp calculated from nucleons (markers) or quarks (lines).

The right part of Fig. 11 shows the results for ρ_{sub} . Results for different β_2 values nearly collapse on a common curve, confirming the earlier statement that these modified quantities are a great way to separate the coefficient b' and c' . The same panels also show the range of the predicted values from Tables I and II. Remarkably, the values from the full Monte Carlo Glauber model agree well with my analytical estimates. The results suggest $\rho_{\text{sub}} = b_0 + c_0 \cos 3\gamma$, with c_0 nearly independent of centrality, while b_0 is roughly constant in 0%–5% centrality and but decreases beyond that.

Repeating the same argument made for $S_{d,\text{sub}}$, the value of ρ_{sub} can be estimated by comparing collisions of two species A and B with similar mass number, therefore canceling the baseline effects. The result is,

$$\rho_{AB} = \frac{\langle \varepsilon_2^2 \frac{\delta d_\perp}{d_\perp} \rangle_A - \langle \varepsilon_2^2 \frac{\delta d_\perp}{d_\perp} \rangle_B}{(\langle \varepsilon_2^2 \rangle_A - \langle \varepsilon_2^2 \rangle_B) \sqrt{\langle (\frac{\delta d_\perp}{d_\perp})^2 \rangle_A - \langle (\frac{\delta d_\perp}{d_\perp})^2 \rangle_B}} \approx \rho_{\text{sub},A}(\varepsilon_2^2, \frac{\delta d_\perp}{d_\perp}) \left(1 + \frac{3}{2}x^2 - \frac{b' + c' \cos(3\gamma_B)}{b' + c' \cos(3\gamma_A)}x^3 + \frac{15}{8}x^4\right), \quad (22)$$

where I assume $x = \beta_{2B}/\beta_{2A} \ll 1$ and I have ignored the small $\cos(3\gamma)$ terms in $C_d\{2\}$ and $\langle \varepsilon_2^2 \rangle$. The b' and c' are the coefficients for $\langle \varepsilon_2^2 \frac{\delta d_\perp}{d_\perp} \rangle$, which are also expected to be the same for the two nuclei. This approximation is accurate within 5% for $x < 0.5$, and the contribution from x^3 and x^4 terms is less than 5% for $x < 0.3$ (the same also applies for Eq. (20)). They can best done for a pair of isobaric system such as Zr+Zr and Ru+Ru collisions, but could also be used for comparison between Au+Au and U+U systems⁵.

⁵ A small correction is required to precisely cancel the a' term [13]. This can be achieved by focusing on central events with similar multiplicity, where the values of a' are smallest and similar between the two systems.

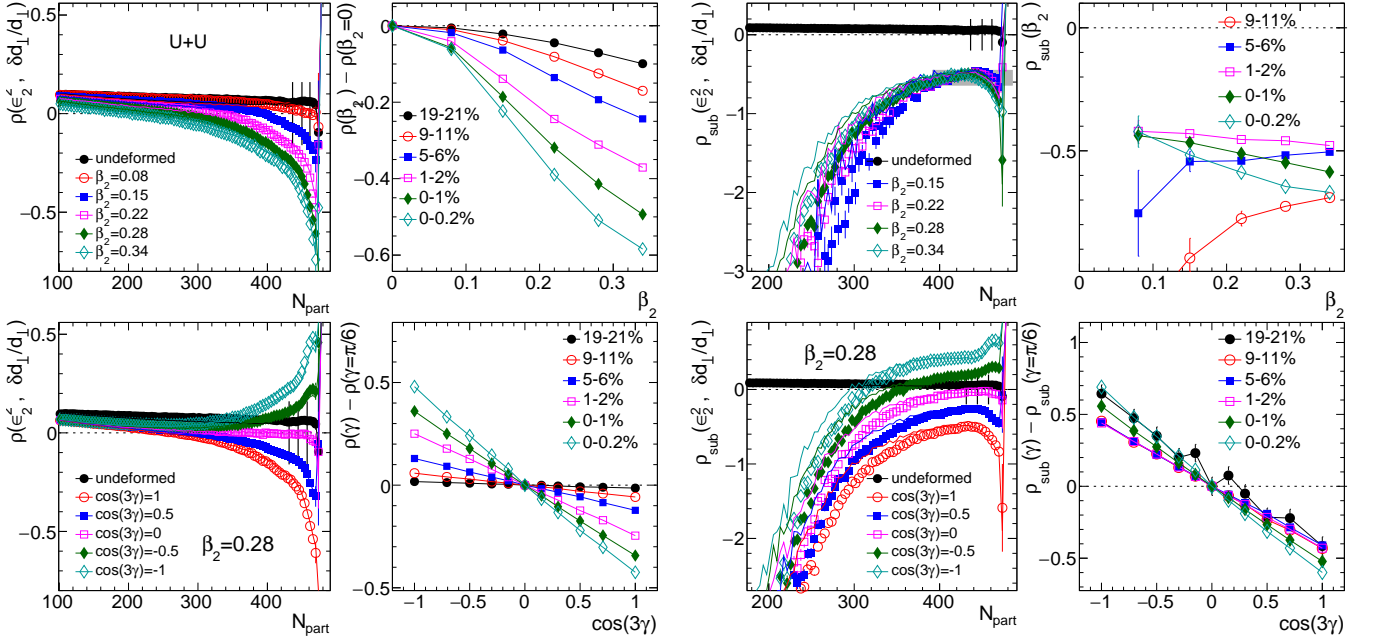


FIG. 11. Left part: The left column shows $\rho(\varepsilon_2^2, \delta d_1/d_1)$ for several β_2 values with $\gamma = 0$ (top row) and for several γ values with $\beta_2 = 0.28$ (bottom row). The left column shows the N_{part} dependence. The right column shows the β_2 (top panel) and $\cos(3\gamma)$ (bottom panel) dependencies. Right part: similar plots for ρ_{sub} , and the shaded band in the top-left panel indicates the predicted range from Tabs. I and II.

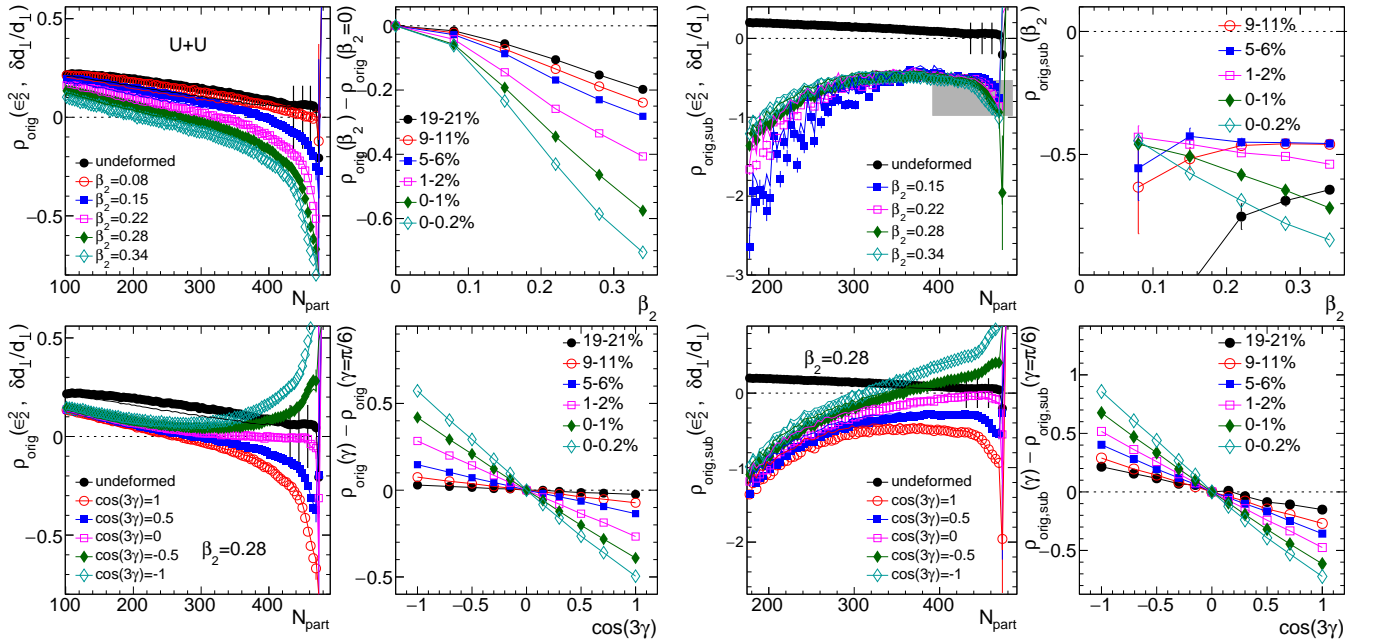


FIG. 12. Same as Fig. 12 but calculated for Pearson correlation coefficients $\rho_{\text{orig}}(\varepsilon_2^2, \delta d_1/d_1)$ defined in Eq. (14).

Although I do not prefer the standard normalization $\rho_{\text{orig}}(\varepsilon_2^2, \delta d_1/d_1)$ for deformation studies, I nevertheless carried out the same calculation since it is widely used before. Here the correlator with the baseline effects subtracted is

defined as

$$\rho_{\text{orig,sub}}(\varepsilon_2^2, \frac{\delta d_\perp}{d_\perp}) = \frac{\langle \varepsilon_2^2 \frac{\delta d_\perp}{d_\perp} \rangle - \langle \varepsilon_2^2 \frac{\delta d_\perp}{d_\perp} \rangle_{\beta_2=0}}{\sqrt{(\langle (\delta \varepsilon_2^2)^2 \rangle - \langle (\delta \varepsilon_2^2)^2 \rangle_{\beta_2=0})(\langle (\frac{\delta d_\perp}{d_\perp})^2 \rangle - \langle (\frac{\delta d_\perp}{d_\perp})^2 \rangle_{\beta_2=0})}} \equiv \rho_{\text{orig}}(\varepsilon_2^2, \frac{\delta d_\perp}{d_\perp})_{\beta_2=\infty}, \quad (23)$$

I shall present the final results in Fig. 12 without detailed discussion. The values and trends in the UCC region are quantitatively similar to ρ_{sub} . This is expected since in central collisions, $c_{2,\varepsilon}\{4\}$ approaches zero and $\langle (\delta \varepsilon_2^2)^2 \rangle \approx \langle \varepsilon_2^2 \rangle^2$, therefore, $\rho_{\text{orig,sub}} \approx \rho_{\text{sub}}$. In the more peripheral region, the two correlators are quantitatively different. The $\rho_{\text{orig,sub}}$ is relatively flat towards mid-central collisions for prolate deformation with different β_2 , however, its γ dependence is much weaker than that for ρ_{sub} .

D. Effects of volume fluctuations and dependence on centrality and system size

Although d_\perp and ε_2 in each event are calculated using either nucleons or quarks, the cumulants of these quantities so far are obtained via an event averaging procedure based on N_{part} . As mentioned before, the averaging could also be performed over event ensembles classified via N_{quark} . Figure 13 summarizes the coefficients b' and c' as a function of centrality for the five quantities $C_d\{2\}, C_d\{3\}, C_d\{4\}, \langle \varepsilon_2^2 \rangle$ and $\langle \varepsilon_2^2 \delta d_\perp / d_\perp \rangle$. The results based on event averaging via N_{quark} are shown in the right two columns, and the results based on event averaging via N_{part} , already presented before in Figs. 3, 7, 8 and 10, are repeated in the left two columns.

For all observables and in almost all cases, the coefficients are quite consistent between U+U and Zr+Zr. Clear differences between event averaging based on N_{part} and those based on N_{quark} are also visible in the UCC region, reflecting the effects of volume fluctuations. These differences are negligible for $\langle \varepsilon_2^2 \rangle$, but reach up to 20% for $C_d\{2\}$ and $\langle \varepsilon_2^2 \delta d_\perp / d_\perp \rangle$; they are even larger for $C_d\{3\}$, and $C_d\{4\}$. What this means is that by selecting extremely central events, one might introduce a large bias from volume fluctuations on skewness and kurtosis. Therefore, the optimal centrality range to maximize the deformation effects, yet avoid strong volume fluctuations, should not be too narrow. A more reasonable choice would be 0%–1% or 0%–5%. In general, the magnitudes of c' are much smaller than b' , except for skewness $C_d\{3\}$ and $\langle \varepsilon_2^2 \delta d_\perp / d_\perp \rangle$ in central collisions where $|c'| \gg |b'|$. The latter reinforces earlier conclusion that three-particle correlations involving v_2 and $[p_T]$ in heavy ion collisions are sensitive probe of the nuclear triaxiality. In some limited cases such as the b' parameter for $C_d\{3\}$ and $C_d\{4\}$, the results are quantitatively different between the nucleon Glauber model and the quark Glauber model (compare the symbols with the lines), suggesting that the deformation contribution to high-order cumulants of d_\perp are also sensitive to the subnucleon fluctuations.

Table III lists the values of a' , b' and c' from Eq. (17) in the 0%–1% most central collisions for the four cases for calculating the observable and performing event averaging. One sees that the values of a' could differ by up to a factor of 2 among the four cases. From these values, one derives the analytical function form for the (β_2, γ) dependence for each observable, including various normalized cumulants discussed in pervious sections.

V. SUMMARY AND A PROPOSAL

I have shown that the two bulk quantities of the initial overlap of the heavy ion collisions, the ε_2 and d_\perp , which quantifies the quadrupole shape and density gradient (or the inverse size) of the overlap region, respectively, are directly related to the quadrupole deformation parameters (β_2, γ) of the colliding nuclei. Aided by hydrodynamic response in the final state, these initial quantities are transformed into the experimentally measured elliptic flow v_2 and average transverse momentum $[p_T]$ in each event. Using an analytical argument and a Glauber model simulation, I derive analytical relations between the cumulants of ε_2/d_\perp and (β_2, γ) . Remarkably, the variances depend mainly on β_2 (i.e. $\langle \varepsilon_2^2 \rangle, \langle (\delta d_\perp / d_\perp)^2 \rangle \sim a' + b' \beta_2^2$), while the skewness are sensitive to both parameters in a simple factorizable form (i.e. $\langle \varepsilon_2^2 \delta d_\perp / d_\perp \rangle, \langle (\delta d_\perp / d_\perp)^3 \rangle \sim a' + (b' + c' \cos(3\gamma)) \beta_2^3$). Similar analytical relations are naturally expected for final-state observables involving v_2 and $[p_T]$. These robust relations provide an efficient way, via a dedicated system scan, to constrain simultaneously the β_2 and γ of the atomic nuclei.

To illustrate how this can be done, one refers to the results obtained from Glauber model for 0%–1% most central

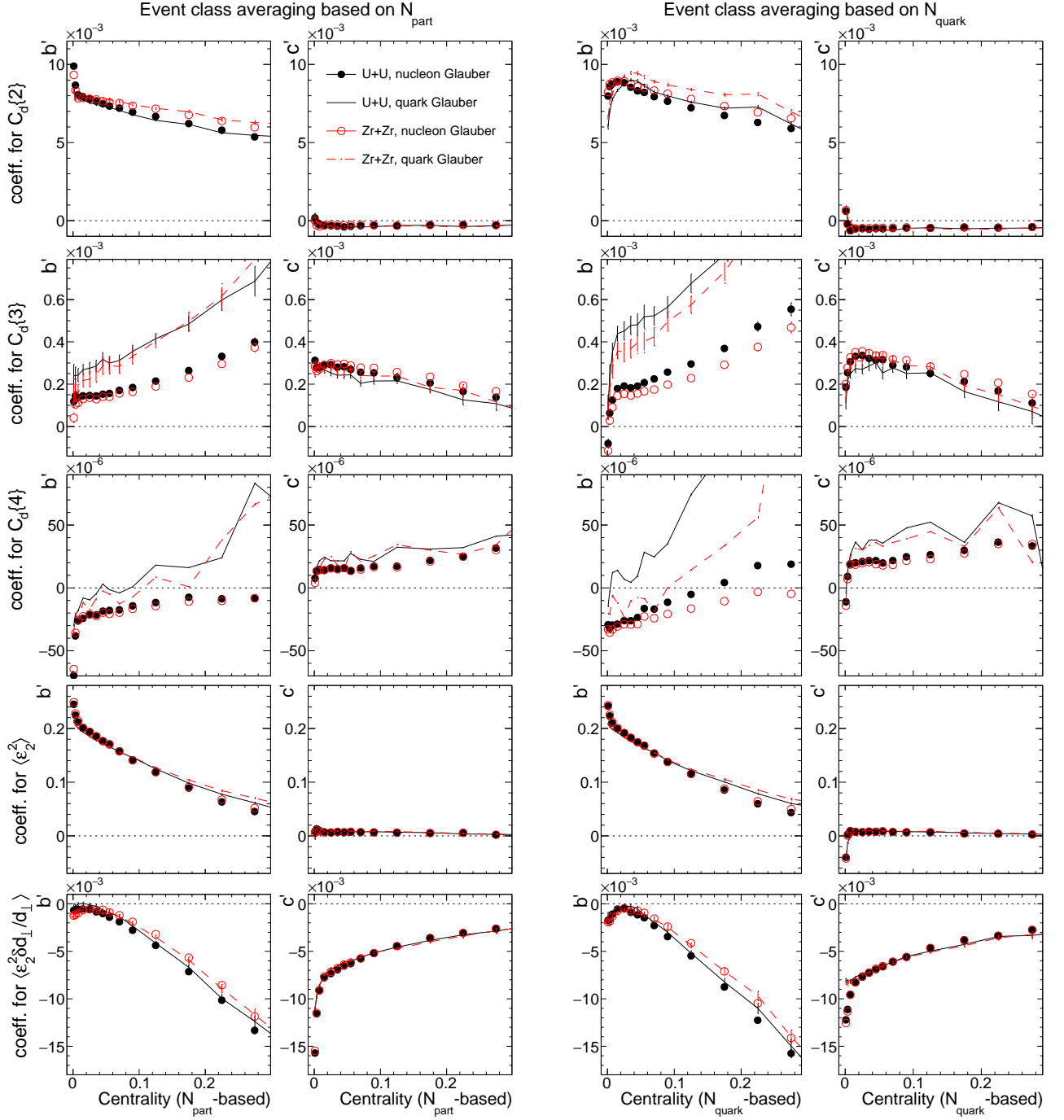


FIG. 13. The centrality dependence of the coefficients b' and c' from Eq. (17) for $C_d\{2\}, C_d\{3\}, C_d\{4\}, \langle \epsilon_2^2 \rangle$ and $\langle \epsilon_2^2 \delta d_\perp / d_\perp \rangle$ from the top row to the bottom row. In each row, the values obtained via event averaging based on N_{part} (left two columns) and N_{quark} (right two columns) are shown. In each panel, the results are compared between U+U and Zr+Zr, and between values calculated from nucleons (symbols) and quarks (lines). The data points for the following centrality ranges are plotted from left to right: 0%–0.2%, 0.2%–0.5%, 0.5%–1%, 1%–2%,..., 5%–6%, 6%–8%, 8%–10%, 10%–15%,..., and 25%–30%.

variable calculation event class	nucleon N_{part}			quark N_{part}			nucleon N_{quark}			quark N_{quark}		
	a'	b'	c'	a'	b'	c'	a'	b'	c'	a'	b'	c'
$\left\langle \left(\frac{\delta d_{\perp}}{d_{\perp}} \right)^2 \right\rangle \times 10^2$ $a' + (b' + c' \cos(3\gamma))\beta_2^2$	0.033	0.93	0.0039	0.038	0.88	-0.015	0.039	0.83	0.019	0.04	0.85	0.023
$\left\langle \left(\frac{\delta d_{\perp}}{d_{\perp}} \right)^3 \right\rangle \times 10^4$ $a' + (b' + c' \cos(3\gamma))\beta_2^3$	0.006	1.3	3.0	0.0084	0.72	2.7	0.012	-0.087	2.2	0.0085	-0.43	2.4
$\left\langle \left(\frac{\delta d_{\perp}}{d_{\perp}} \right)^4 \right\rangle - 3 \left\langle \left(\frac{\delta d_{\perp}}{d_{\perp}} \right)^2 \right\rangle^2 \times 10^5$ $a' + (b' + c' \cos(3\gamma))\beta_2^4$	0.00033	-5.4	1.1	0.00065	-5.0	0.88	0.00064	-3.1	-0.1	0.00052	-3.4	-0.35
$\langle \varepsilon_2^2 \rangle \times 10$ $a' + (b' + c' \cos(3\gamma))\beta_2^2$	0.045	2.35	0.11	0.055	2.38	0.083	0.047	2.32	-0.19	0.056	2.34	-0.21
$\left\langle \varepsilon_2^2 \frac{\delta d_{\perp}}{d_{\perp}} \right\rangle \times 10^2$ $a' + (b' + c' \cos(3\gamma))\beta_2^3$	0.00051	-0.066	-1.36	0.00070	-0.12	-1.35	0.00097	-0.17	-1.17	0.00084	-0.19	-1.19

TABLE III. The values of the coefficients a' , b' and c' of Eq. (17) for each observable in 0–1% U+U collisions from the Glauber model. They are listed for four cases: variables can be calculated with either nucleons or quarks and the event averaging are also based on either nucleons or quarks.

U+U collisions from the first column of Tab. III,

$$\begin{aligned}
\langle \varepsilon_2^2 \rangle &\approx [0.02 + \beta_2^2] \times 0.235 \\
\langle (\delta d_{\perp}/d_{\perp})^2 \rangle &\approx [0.035 + \beta_2^2] \times 0.0093 \\
\langle (\delta d_{\perp}/d_{\perp})^3 \rangle &\approx [0.006 + (1.3 + 3.0 \cos(3\gamma))\beta_2^3] \times 10^{-4} \\
\langle \varepsilon_2^2 \delta d_{\perp}/d_{\perp} \rangle &\approx [0.0005 - (0.07 + 1.36 \cos(3\gamma))\beta_2^3] \times 10^{-2}
\end{aligned} \tag{24}$$

From these I construct ratios $\rho(\varepsilon_2^2, \delta d_{\perp}/d_{\perp})$ and S_d , as well as baseline subtracted ratios ρ_{sub} and $S_{d,\text{sub}}$ (their definitions are repeated in Fig. 14). Eq. (24) can map any trajectory in the (β_2, γ) diagram from low-energy nuclear structure side (so-called ‘‘Hill-Wheeler’’ coordinate) onto new trajectories in various correlation plots from high-energy side as shown in the bottom panels (a)–(f). I note that the direction of the trajectory in the $(\rho, \langle \varepsilon_2^2 \rangle)$ plane is opposite to that in the $(S_d, \langle \varepsilon_2^2 \rangle)$ plane, and the trajectory in the (ρ, S_d) plane almost collapses into a straight line. The γ dependences in these plots follow a simple linear function of $\cos(3\gamma)$, while the β_2 dependence is more complex due to the offsets in Eq. (24). The correlations are much well behaved for ρ_{sub} and $S_{d,\text{sub}}$ as shown in the bottom row of Fig. 14. In particular, the differences between prolate and oblate deformation for these quantities are independent of β_2 , and they are also expected to be nearly independent of centrality as suggested by Figs. 9 and 11. Therefore, one could determine the γ angle of any nucleus with similar mass number, once the values of ρ_{sub} and S_{sub} are calibrated from collisions of prolate and oblate nuclei with known β_2 .

A few additional summarizing points can be made about these flow diagrams. 1) One can replace the x -axis with $\langle (\delta d_{\perp}/d_{\perp})^2 \rangle$, the trajectories would be shifted and rescaled but their shapes remain the same. 2) Since the coefficients b' and c' are relatively insensitive to the size of the collision systems, the correlations in the bottom row of Fig. 14 are expected to be valid for all medium and large nuclei. By the way, the change of ρ_{sub} and $S_{d,\text{sub}}$ when nuclear shape is varied from prolate to oblate, unlike ρ and S_d , are also relatively independent of centrality. This implies that the curves in the bottom panels only shift vertically and narrow horizontally for events in mid-central collisions, but the height remains roughly the same. 3) One should be able to construct similar flow diagrams for cumulants of v_2 and $[p_T]$ in the final state. This can be estimated from the well-known linear relation $v_2 \propto \varepsilon_2$ and $\delta[p_T]/[p_T] \propto \delta d_{\perp}/d_{\perp}$, or more precisely evaluated from the full hydrodynamic model simulations. 4) The generalization of this idea to kurtosis and higher-order cumulants may not work well due to strong nonlinear mode mixing from lower-order cumulants.

Study of the nuclear deformation, in particular shape evolution in the (β_2, γ) diagram along the isobaric chain by adding neutron and protons, is one of the most important areas of research in nuclear structure community [1].

$\beta_2 - \gamma$ Diagram in Heavy-ion Collisions

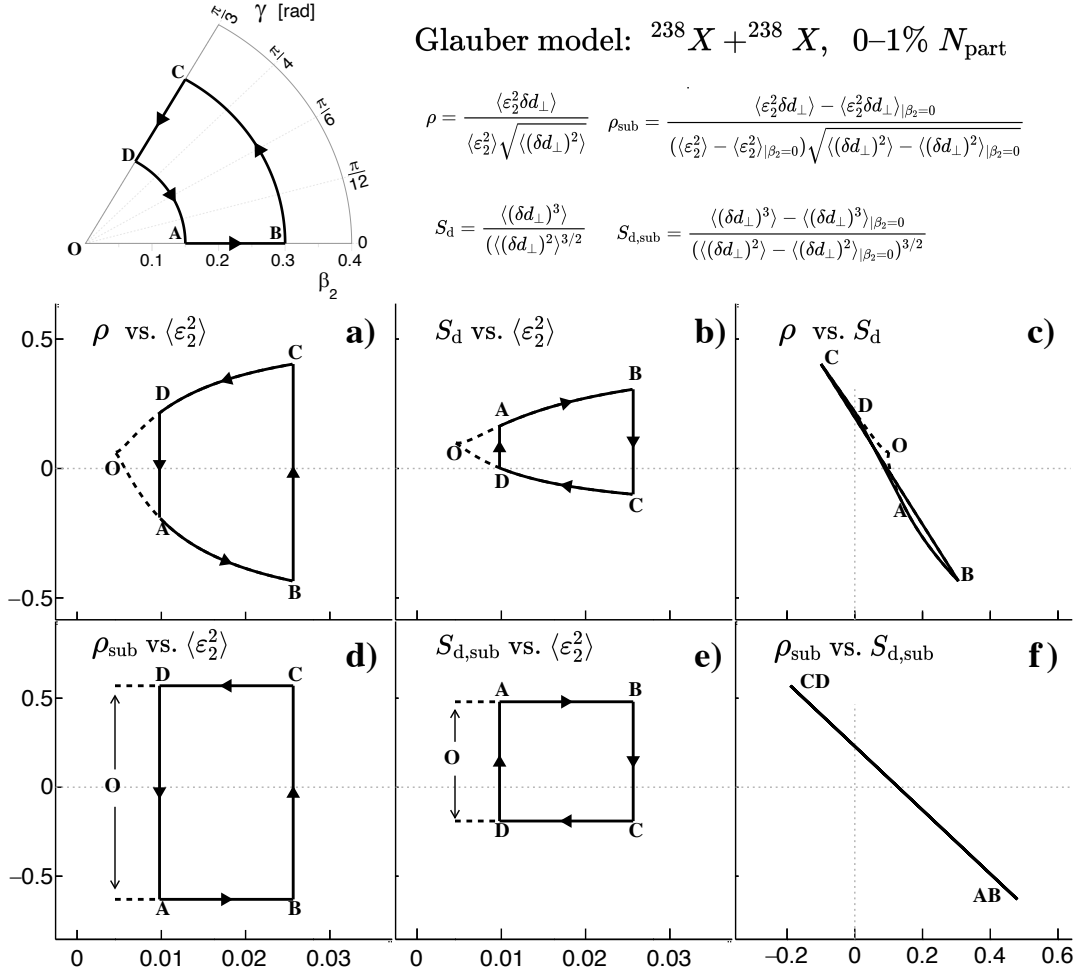


FIG. 14. Glauber model prediction of the mapping of a closed trajectory on the (β_2, γ) plane from nuclear structure side (top-left) onto a trajectory on the $(\rho, \langle \varepsilon_2^2 \rangle)$ plane (panel-a), the $(S_d, \langle \varepsilon_2^2 \rangle)$ plane (panel-b), as well as that for the baseline-subtracted quantity $(\rho_{\text{sub}}, \langle \varepsilon_2^2 \rangle)$ (panel-d) and $(S_{d,\text{sub}}, \langle \varepsilon_2^2 \rangle)$ (panel-e). The definition of these quantities are given in the top-right corner. The trajectories are also shown on the (ρ, S_d) plane (panel-c) and on the $(\rho_{\text{sub}}, S_{d,\text{sub}})$ plane (panel-f). The results are shown for collision of nucleus with 238 nucleons and for the 0%–1% most central events selected based on N_{part} . Note that the correlation with variance $\langle (\delta d_{\perp}/d_{\perp})^2 \rangle$ as the x -axis are similar, i.e. only require a shift and rescaling (see text).

High-energy heavy-ion collisions offer a new tool to image the shape of atomic nuclei by smashing them together and measure the collective flow response in the final state. The skewness $\langle (\delta d_{\perp}/d_{\perp})^3 \rangle$ and $\langle \varepsilon_2^2 \delta d_{\perp}/d_{\perp} \rangle$, experimentally accessible via three-particle correlations $\langle (\delta[p_{\text{T}}]/[p_{\text{T}}])^3 \rangle$ and $\langle v_2^2 \delta[p_{\text{T}}]/[p_{\text{T}}] \rangle$, show remarkably strong sensitivity to triaxiality over a broad range of centrality, as well as nearly system-size independent signal strength. The existing data from various species, in particular the recent isobar $^{96}\text{Zr} + ^{96}\text{Zr}$ and $^{96}\text{Ru} + ^{96}\text{Ru}$ collision data [51] at high energy, provide a unique opportunity to test the methodology proposed in this paper [53, 54]. However, most valuable information will ultimately arise from a collision scan of systems for which one already have precision knowledge from the nuclear structure community to calibration the hydrodynamic response, followed by application to systems for which one not have sufficient understanding.

Acknowledgements: I am grateful for the AMPT simulation data provided by Chunjian Zhang. I thank Giuliano Giacalone, Chunjian Zhang and Somadutta Bhatta for valuable discussions. This work is supported by DOE DEFG0287ER40331.

Appendix A: AMPT model

I have shown that the initial state of the heavy ion collisions are very sensitive to quadrupole deformation and triaxiality of the colliding nuclei, and I have constructed multiple observables to constrain β_2 and γ independently. The next crucial question, however, is how much of these sensitivities in the initial state survive to the particle correlations in the final state. Previous hydrodynamic model studies and data comparisons have firmly established the proportionality between ε_2 and v_2 , and to lesser extent also the positive correlation between d_\perp and $[p_T]$ [28, 55] and between $\langle \varepsilon_2^2, \delta d_\perp \rangle$ and $\langle v_2^2, \delta[p_T] \rangle$ [29, 56].

To understand the conversion from ε_2 and d_\perp in the initial overlap to v_2 and $[p_T]$ in the final state, the popular event generator ‘‘a multi-phase transport model’’ (AMPT) [57] is used, which is a realistic yet computationally efficient way to implement hydrodynamic response. The AMPT model has been demonstrated to qualitatively describe the harmonic flow v_n in p +A and A+A collisions [58, 59], so it can be used to predict the β_2 dependence of v_n . A previous study has demonstrated a robust simple quadratic dependence $\langle v_2^2 \rangle = a + b\beta_2^2$ in the final state as a result of a linear response to a similar dependence in the initial state $\langle \varepsilon_2^2 \rangle = a' + b'\beta_2^2$ [13, 14]. However this model is known to have the wrong hydrodynamic response for the radial flow, i.e. the centrality dependence of average transverse momentum $\langle p_T \rangle \equiv \langle [p_T] \rangle$ and the variance $\langle (\delta[p_T])^2 \rangle$ do not describe the experimental data [14, 49]. A recent modification of the model [60] fixed the problem with the $\langle p_T \rangle$, but the value of $\langle (\delta[p_T])^2 \rangle$ is still more than a factor of 3 lower than the STAR data [21, 61]⁶. This implies that the response of $[p_T]$ to d_\perp in AMPT is a lot weaker than the experimental finding, and explains why the model fails to describe quantitatively the behavior of $\langle v_2^2 \delta[p_T] \rangle$ in U+U collisions observed in the STAR data [21]. Nevertheless, since the response of v_2 is correct, one can still study the parametric (β_2, γ) dependence of $\langle v_2^2 \delta[p_T] \rangle$ and compare with the trend of $\langle \varepsilon_2^2 \delta d_\perp \rangle$. However, this unfortunately can not be said about cumulants of $[p_T]$ fluctuations.

Following Refs [63–65], I use the AMPT model v2.26t5 with string-melting mode and partonic cross section of 3.0 mb, which I check reasonably reproduce Au+Au v_2 data at RHIC. The Woods-Saxon parameters in the AMPT are chosen to be $R_0 = 6.81$ fm and $a = 0.54$ similar to [6] but with different fixed values of (β_2, γ) . The v_2 and $[p_T]$ are calculated with all hadrons with $0.2 < p_T < 2$ GeV and $|\eta| < 2$, and the event centrality is defined using either N_{part} or inclusive hadron multiplicity in $|\eta| < 2$, N_{hadron} . The value of N_{hadron} , which include both charged and neutral particles, is about six times of the charged hadron multiplicity density, i.e. $N_{\text{hadron}} \approx 6dN_{\text{ch}}/d\eta$.

One main drawback of the AMPT model is that it underestimates the hydrodynamic response of radial flow. For one thing, it undershoots the variance of the p_T fluctuations from data, see the left panel of Fig. 15. The right panel shows that the AMPT model predicts a very weak dependence of $\langle (\delta[p_T]/[p_T])^2 \rangle$ on β_2 . Even for a value of $\beta_2 = 0.28$, the increase of $[p_T]$ variance is only 30%. Similar observation is also made for $\langle (\delta[p_T]/[p_T])^3 \rangle$ (not shown). This is in clear contradiction to the much larger influence from deformation observed in the recent experimental results of variance and skewness of $[p_T]$ in U+U and Au+Au collisions [21]. Hence, AMPT model can not be used to study reliably the deformation effects on the $[p_T]$ fluctuations. Instead, I shall focus on $\langle v_2^2 \delta[p_T] \rangle$, the rationale being that even though the radial flow response is underestimated, the elliptic flow response is still correctly modeled. I hope to at least explore the qualitative features of $\langle v_2^2 \delta[p_T] \rangle$ and compare to $\langle \varepsilon_2^2 \delta d_\perp \rangle$.

The left column of Fig. 16 shows the N_{part} dependence of $\langle v_2^2 \delta[p_T]/[p_T] \rangle$ for several values of β_2 and γ , calculated using the multi-particle correlation framework of Ref. [66]. There are clear sensitivity on both parameters, especially in the UCC region. The values are integrated over several centrality ranges and plotted as a function of β_2^3 and $\cos(3\gamma)$ in the middle column, calculated from the corresponding data in the left column. Despite the large statistical uncertainties, linear dependences are observed, confirming the trends seen in the Glauber model:

$$\langle v_2^2 (\delta[p_T]/[p_T]) \rangle = a + (b + c \cos(3\gamma)) \beta_2^3. \quad (\text{A1})$$

The values of b and c are shown in the right column as a function of centrality; the centrality-dependent trends are similar to those obtained from Glauber model (compare to Fig. 10). However, the values of b and c are about a factor of 100 smaller than b' and c' , also b is larger than 0 in central collisions, while b' is less than 0 over the full centrality range. In hydrodynamic model with linear response assumption of Eq. (4), one has approximately,

$$\left\langle v_2^2 \frac{\delta[p_T]}{[p_T]} \right\rangle \approx k_2^2 k_0 \left\langle \varepsilon_2^2 \frac{\delta d_\perp}{d_\perp} \right\rangle \quad (\text{A2})$$

Using the value of $k_2 \approx 0.2$ from a hydrodynamic model [67] and $k_0 \approx 0.4$ from left panel of Fig. 11 in central collisions, one expects a factor of 60. I also repeat the same analysis using N_{hadron} to classify events. They give very

⁶ Hydrodynamic model simulation based on Trento initial condition [62] predicts a much larger $[p_T]$ fluctuation, but with very little sensitivity on β_2 .

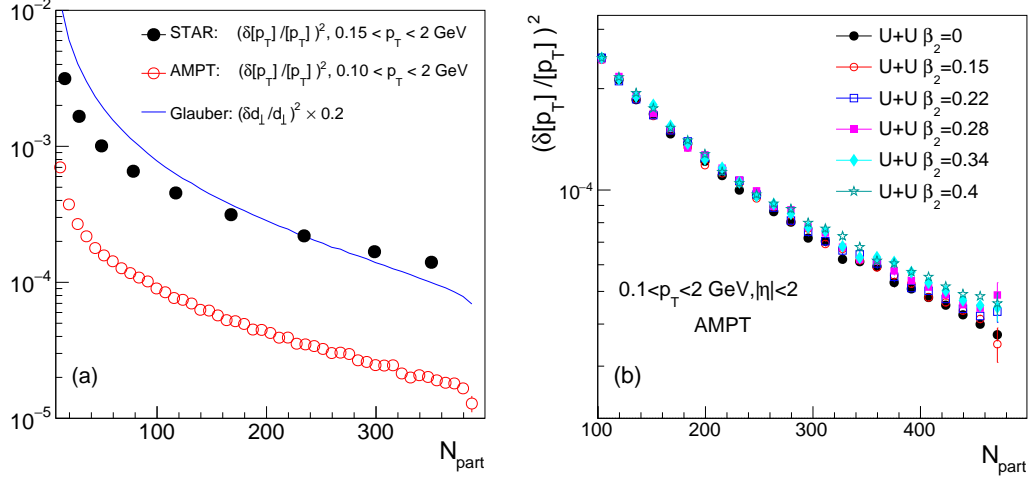


FIG. 15. Left: variance of $[p_T]$ fluctuation from AMPT model (open symbol) and experimental data Ref. [61] (solid symbol), as well as the variance of d_L (solid line) in Au+Au collisions at $\sqrt{s_{NN}} = 200$ GeV. Right: variance of $[p_T]$ from AMPT model in U+U collisions for different values of β_2 .

similar values of b and c as shown in the right column of Fig. 16, implying the results are robust against the volume fluctuations.

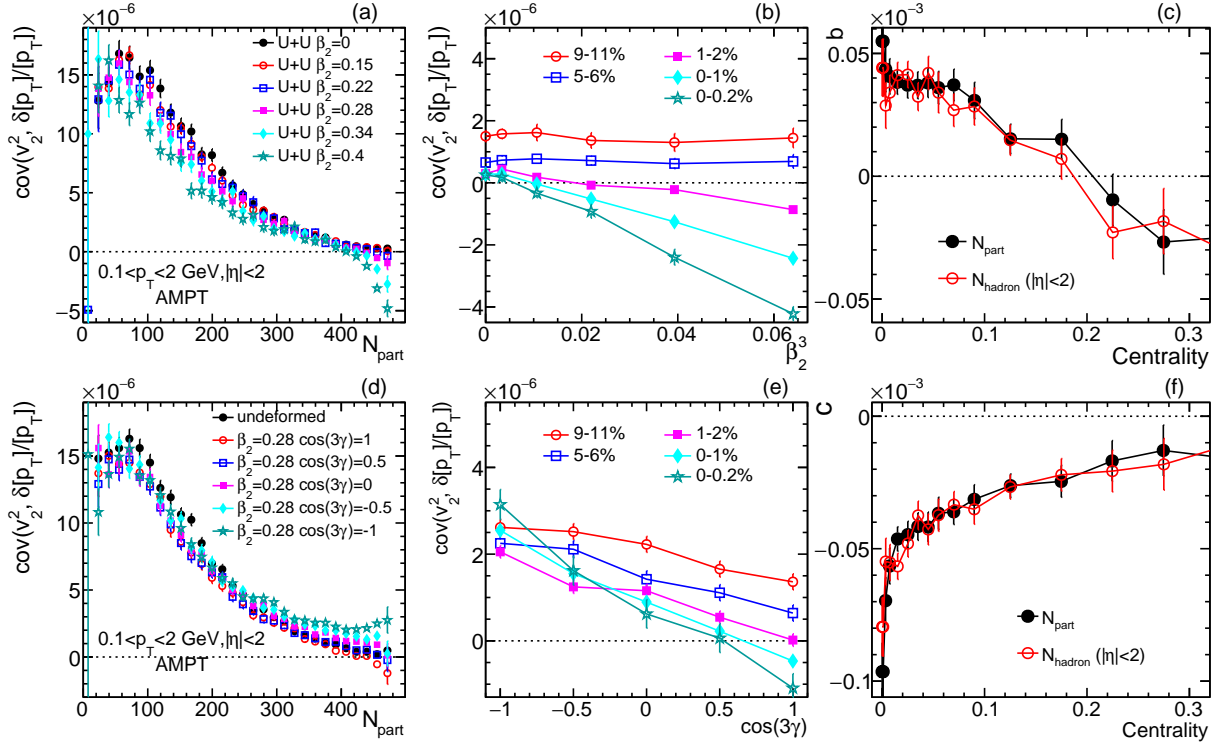


FIG. 16. The $\langle v_2^2 \delta[p_T]/[p_T] \rangle$ for several β_2 values of prolate shape $\gamma = 0$ (top row) and several γ values with $\beta_2 = 0.28$ (bottom row) in U+U collisions from the AMPT model. The left column show the N_{part} dependence. The middle column shows the results as a function of β_2^3 (top panel) or $\cos(3\gamma)$ (bottom panel) in several centrality ranges based on N_{part} . The right column summarizes the coefficients b (top) and c (bottom) from Eq. (A1) as a function of centrality based on N_{part} (filled symbols) or N_{hadron} (open symbols).

From these results, I calculate the normalized quantities, $\rho(v_2^2, \frac{\delta[p_T]}{[p_T]})$ and $\rho_{sub}(v_2^2, \frac{\delta[p_T]}{[p_T]})$, defined similar to those

in Eqs. (14) and (21). The results are shown in Fig. 17 for β_2 dependence on the left part and γ dependence on the right part. The ρ follows approximately a linear dependence of β_2 , similar to Glauber model results (top panel in the second column of Fig. 11). The ρ_{sub} in the bottom panels are nearly independent of β_2 as expected. For the $\cos(3\gamma)$ dependence, ρ data exhibit different slopes for different centralities ranges, but ρ_{sub} data follow a common slope in all centrality ranges. What this means is that the difference of ρ_{sub} between prolate and oblate is approximately independent of centrality, similar to the results from Glauber model shown in the bottom right panel of Fig. 11.

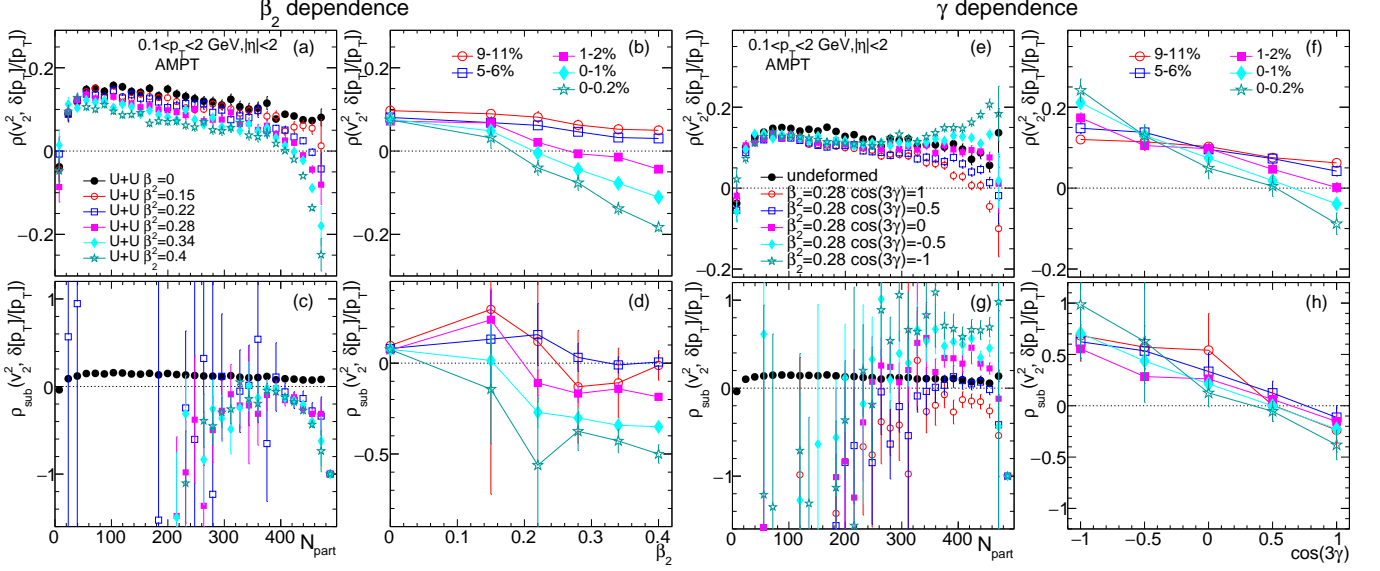


FIG. 17. Left Part: The $\rho(v_2^2, \delta[p_T]/[p_T])$ (top row) and $\rho_{\text{sub}}(v_2^2, \delta[p_T]/[p_T])$ (bottom row) as a function of N_{part} for several β_2 values of prolate shape $\gamma = 0$ (left column) and as a function of β_2 in several centrality ranges based on N_{part} (right column). Right part: The $\rho(v_2^2, \delta[p_T]/[p_T])$ (top row) and $\rho_{\text{sub}}(v_2^2, \delta[p_T]/[p_T])$ (bottom row) as a function of N_{part} for several γ values with $\beta_2 = 0.28$ (left column) and as a function of $\cos(3\gamma)$ in several centrality ranges based on N_{part} (right column).

Appendix B: Transverse size fluctuations in head-on collisions

Although the shape and size of atomic nuclei with static deformation is fixed in the intrinsic frame, the shape and size for the distribution projected to the transverse plane (x, y) in the laboratory frame depend on the Euler angle Ω , and therefore fluctuates event to event. The expression for ϵ_2 has been derived in the Appendix A of Ref. [15], I shall focus on $\delta d_{\perp}/d_{\perp}$ in Eq. (11).

First, I express the angular weights of variance and covariance of the coordinates, $\langle x^2 \rangle = \langle r^2 \sin^2 \theta \sin^2 \phi \rangle$, $\langle y^2 \rangle = \langle r^2 \sin^2 \theta \cos^2 \phi \rangle$ and $\langle xy \rangle = \langle r^2 \sin^2 \theta \sin \phi \cos \phi \rangle$ in terms of spherical harmonics,

$$\begin{aligned} \sin^2 \theta \cos^2 \phi &= \frac{1}{3} + \sqrt{\frac{2\pi}{15}} (Y_2^2 + Y_2^{-2}) - \frac{2}{3} \sqrt{\frac{\pi}{5}} Y_2^0, & \sin^2 \theta \sin^2 \phi &= \frac{1}{3} - \sqrt{\frac{2\pi}{15}} (Y_2^2 + Y_2^{-2}) - \frac{2}{3} \sqrt{\frac{\pi}{5}} Y_2^0, \\ \sin^2 \theta \sin \phi \cos \phi &= -i \sqrt{\frac{2\pi}{15}} (Y_2^2 - Y_2^{-2}). \end{aligned} \quad (\text{B1})$$

In the rotated frame, one needs to apply the substitution $Y_2^m \rightarrow \sum_{m'} D_{m, m'}^2(\Omega) Y_2^{m'}$. Keeping the leading order term in β_2 , using the notation $\alpha_0 = \cos \gamma$, $\alpha_2 = \alpha_{-2} = \sin \gamma / \sqrt{2}$ for quadrupole deformation, the variances and covariance

become

$$\langle x^2, y^2 \rangle = \frac{\int \rho(r) r^4 dr \int (1 + \beta_2 \sum_m \alpha_m Y_2^m)^5 \left[\frac{1}{3} \pm \sqrt{\frac{2\pi}{15}} \sum_{m'} (D_{2,m'}^2 + D_{-2,m'}^2) Y_2^{m'} - \frac{2}{3} \sqrt{\frac{\pi}{5}} \sum_{m'} D_{0,m'}^2 Y_2^{m'} \right] \sin \theta d\theta d\phi}{\int \rho(r) r^2 dr \int (1 + \beta_2 \sum_m \alpha_m Y_2^m)^3 \sin \theta d\theta d\phi}$$

$$\approx \frac{R_0^2}{5} \left[1 + \sqrt{\frac{5}{4\pi}} \beta_2 \sum_{m'} \alpha_{m'} \left(-\sum_{m'} D_{0,m'}^2 \pm \sqrt{\frac{3}{2}} (D_{2,m'}^2 + D_{-2,m'}^2) \right) \right] \quad (\text{B2})$$

$$\langle xy \rangle \approx -i \frac{R_0^2}{5} \frac{15\beta_2}{4\pi} \sum_{m'} \alpha_{m'} (D_{2,m'}^2 - D_{-2,m'}^2). \quad (\text{B3})$$

The transverse area S_\perp in the projected plane has the following expression

$$\frac{S_\perp^2}{\pi^2} = \langle x^2 \rangle \langle y^2 \rangle - \langle xy \rangle^2 = \frac{R_0^4}{25} \left[1 - \sqrt{\frac{5}{\pi}} \beta_2 \sum_m \alpha_m D_{0,m}^2 + \frac{5}{4\pi} \beta_2^2 \sum_{m,m'} \alpha_m \alpha_{m'} (D_{0,m}^2 D_{0,m'}^2 - 6D_{2,m}^2 D_{-2,m'}^2) \right] \quad (\text{B4})$$

Keeping the leading term β_2 , the fluctuation relative to the averaging over the Ω is

$$\frac{\delta d_\perp}{d_\perp} = -\frac{1}{4} \frac{\delta S_\perp^2}{S_\perp^2} = \sqrt{\frac{5}{16\pi}} \beta_2 \sum_m \alpha_m D_{0,m}^2 = \sqrt{\frac{5}{16\pi}} \beta_2 \left(\cos \gamma D_{0,0}^2 + \frac{\sin \gamma}{\sqrt{2}} [D_{0,2}^2 + D_{0,-2}^2] \right), \quad (\text{B5})$$

where I have used the relation $d_\perp = \sqrt{N_{\text{part}}/S_\perp}$ and assumed N_{part} is a constant in head-on collisions.

Two comments are in order. First, the transverse area can also be defined as $S_\perp = \pi (\langle x^2 \rangle + \langle y^2 \rangle)$. This definition gives exactly the same expression for $\delta d_\perp/d_\perp$ in the leading order of β_2 . Second, in general the next-leading order contribution to d_\perp contains terms that scale like $\beta_2^2 (\sum_m \alpha_m D_{0,m}^2)^2$ or $\beta_2^2 (\sum_m \alpha_m D_{2,m}^2) (\sum_m \alpha_m D_{2,m}^2)^*$. In the calculation of variances, they will appear as

$$\begin{aligned} \langle (\delta d_\perp/d_\perp)^2 \rangle &= \frac{5}{16\pi} \langle (\beta_2 \Sigma + c_1 \beta_2^2 \Sigma^2 + c_2 \beta_2^2 \Pi^2 + \mathcal{O}(\beta_2^3))^2 \rangle = \frac{5}{16\pi} \beta_2^2 [\langle \Sigma^2 \rangle + 2c_1 \beta_2 \langle \Sigma^3 \rangle + 2c_2 \beta_2 \langle \Sigma \Pi^2 \rangle + \mathcal{O}(\beta_2^2)] \\ &= \frac{1}{16\pi} \beta_2^2 \left(1 + \frac{4}{7} (c_1 - c_2) \beta_2 \cos(3\gamma) + \mathcal{O}(\beta_2^2) \right) \end{aligned} \quad (\text{B6})$$

where I denote $\Sigma \equiv \sum_m \alpha_m D_{0,m}^2$ and $\Pi^2 \equiv (\sum_m \alpha_m D_{2,m}^2) (\sum_m \alpha_m D_{2,m}^2)^*$, and the values of c_1 and c_2 depend on the definition of d_\perp . For the case in Eq. (B4), one can show $c_2 = \frac{2}{3} c_1 = \frac{3}{2} \sqrt{\frac{5}{16\pi}} = 0.473$. The two higher-order terms in this expansion have the same form as those in Eq. (12), and their contributions are proportional to $\cos(3\gamma)$. They are responsible for the clear residual dependence on the triaxiality of $\langle (\delta d_\perp/d_\perp)^2 \rangle$ in Fig. 5 and $\langle \varepsilon_2^2 \rangle$ in Ref. [15]. That is why the prolate deformation with $\beta_2 = 0.28$ in the left panels of Fig. 5 has a smaller $\langle (\delta d_\perp/d_\perp)^2 \rangle$ value by about $8/7(c_1 - c_2)\beta_2 = 7\%$ in central collisions.

Following Eq. (B6), one can also estimate the higher-order correction to the skewness and kurtosis

$$\begin{aligned} \langle (\delta d_\perp/d_\perp)^3 \rangle &= \left(\frac{5}{16\pi} \right)^{3/2} \langle (\beta_2 \Sigma + c_1 \beta_2^2 \Sigma^2 + c_2 \beta_2^2 \Pi^2)^3 \rangle = \left(\frac{5}{16\pi} \right)^{3/2} \beta_2^3 [\langle \Sigma^3 \rangle + 3c_1 \beta_2 \langle \Sigma^4 \rangle + 3c_2 \beta_2 \langle \Sigma^2 \Pi^2 \rangle] \\ &= \frac{\sqrt{5}}{224\pi^{3/2}} \beta_2^3 \left(\cos(3\gamma) + \frac{9c_1 + 3c_2}{2} \beta_2 \right) \end{aligned} \quad (\text{B7})$$

$$\begin{aligned} \langle (\delta d_\perp/d_\perp)^4 \rangle - 3 \langle (\delta d_\perp/d_\perp)^2 \rangle^2 &= \frac{5}{16\pi} \beta_2^4 [\langle \Sigma^4 \rangle - 3 \langle \Sigma^2 \rangle^2 + 4\beta_2 (c_1 \langle \Sigma^5 \rangle + c_2 \langle \Sigma^3 \Pi^2 \rangle - 3c_1 \langle \Sigma^2 \rangle \langle \Sigma^3 \rangle - 3c_2 \langle \Sigma^2 \rangle \langle \Sigma \Pi^2 \rangle)] \\ &= \frac{3}{896\pi^2} \beta_2^4 \left(-1 + \frac{4}{33} (17c_1 + 23c_2) \beta_2 \cos(3\gamma) \right) \end{aligned} \quad (\text{B8})$$

For skewness, the higher-order term leads to a positive shift for S_d . For $\beta_2 = 0.28$, it is $\Delta S_d/|S_d| = \frac{9c_1 + 3c_2}{2} \beta_2 = 2.2$, i.e. the amount of shift is comparable to the variation from prolate and oblate deformation. In reality, one observe the shift is about 1/3 of the predicted size (see bottom-left panel of Fig. 7). For kurtosis, the contribution is about $\Delta K_d/|K_d| = \frac{4}{33} (17c_1 + 33c_2) \beta_2 \cos 3\gamma \approx 0.79 \cos 3\gamma$. Assuming $K_d = -3/7$ from Tab. II, then $\Delta K_d = 0.33 \cos 3\gamma$, which is about a factor of 3 of what is observed in the Glauber model (top-right panel of Fig. 9).

Appendix C: Additional plots

This appendix shows comprehensive centrality dependence of various observables for different values of β_2 and γ used in the paper in U+U and Zr+Zr collisions. The full set of observables for the cumulants of d_\perp are shown in Fig. 18 for U+U and Fig. 19 for Zr+Zr, respectively. Similarly, information for $\langle \varepsilon_2^2 \rangle$ and correlation between ε_2 and d_\perp are shown in Figs. 20 and 21. Most importantly these plots show the results obtained with the N_{quark} -based event averaging. See also Figs. 22 and 23.

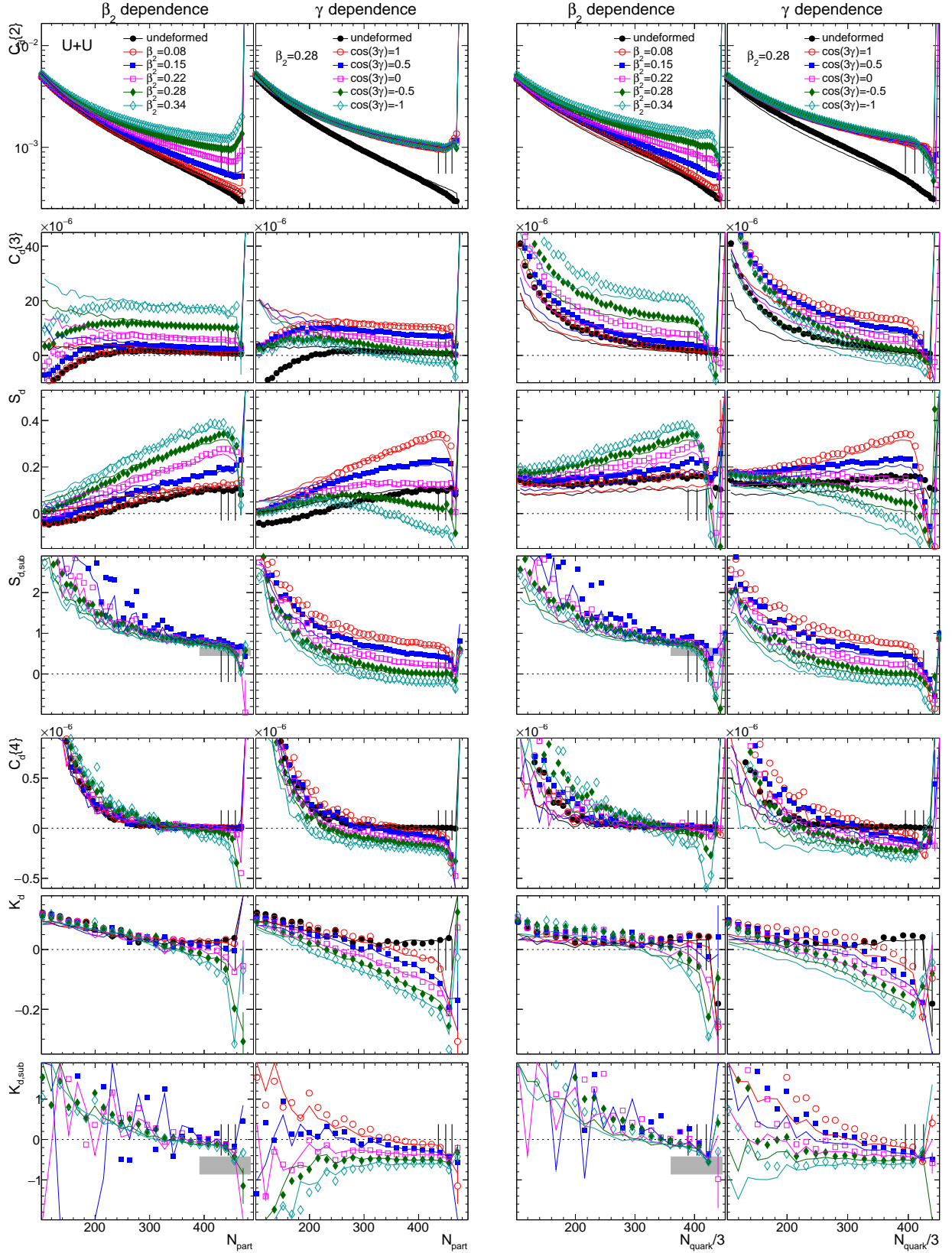


FIG. 18. N_{part} (left two columns) and N_{quark} (right two columns) dependences of various d_1 observables as indicated by the y -axis title in the left side, in U+U collisions compared between different β_2 (1st and 3rd columns) and different γ with $\beta_2 = 0.28$ (2nd and 4th columns), calculated with nucleons (symbols) and quarks (lines). The vertical lines in each panel correspond to locations for 0.2%, 1% and 2% centralities.

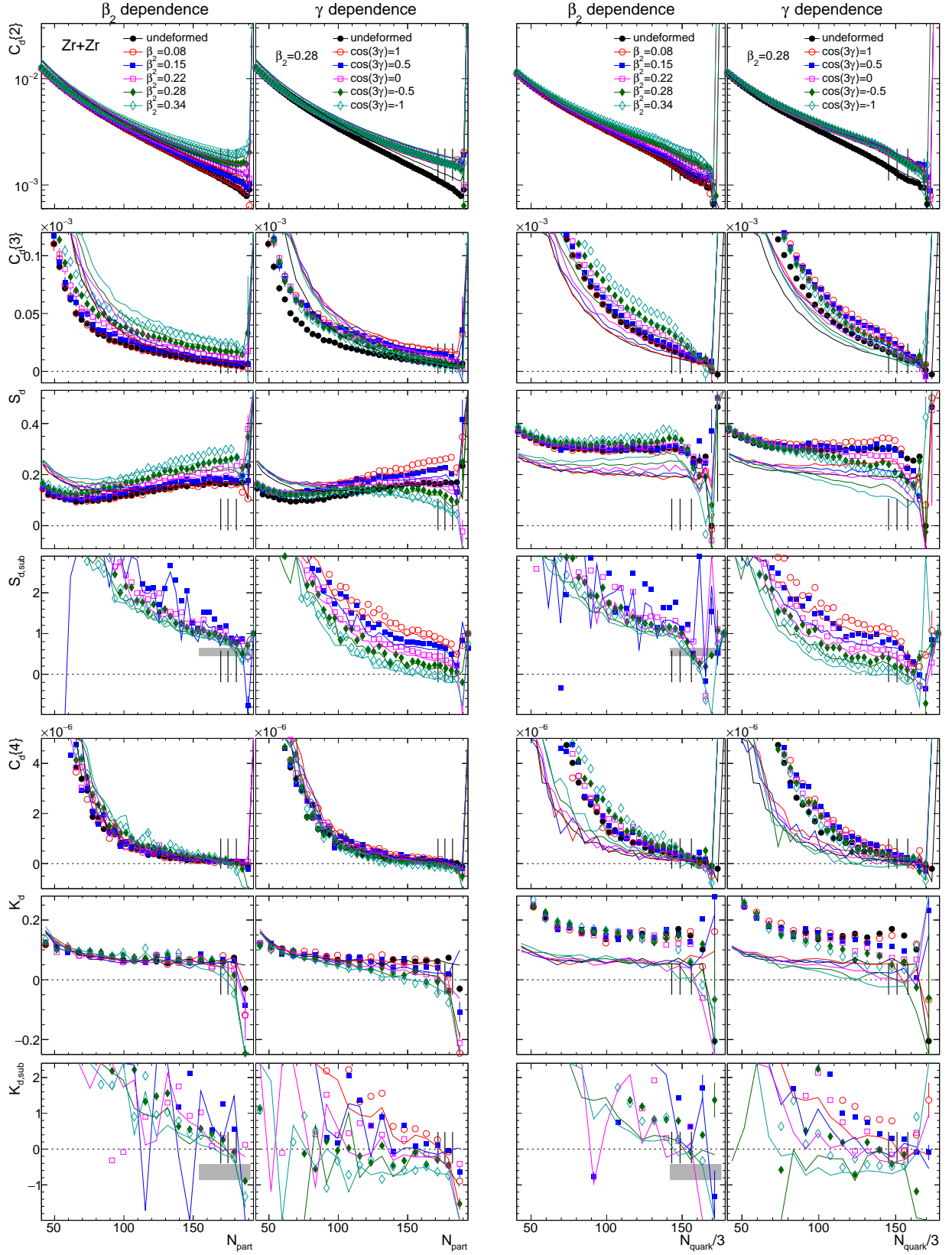


FIG. 19. Same as Fig. 18 but for Zr+Zr collisions.

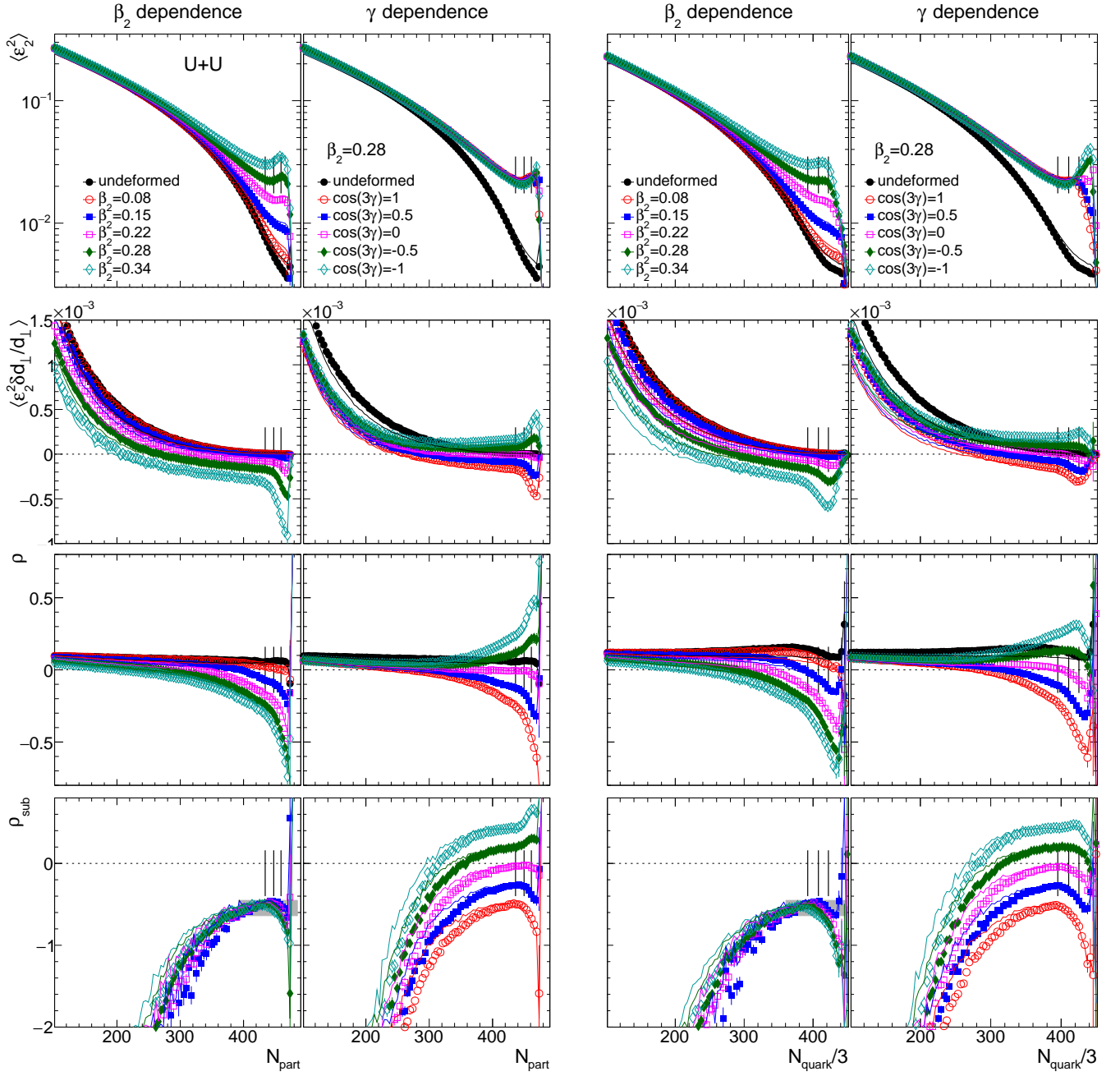


FIG. 20. N_{part} (left two columns) and N_{quark} (right two columns) dependencies of various observables related to ε_2 in U+U collisions compared between different β_2 (1st and 3rd columns) and different γ with $\beta_2 = 0.28$ (2nd and 4th columns), calculated with nucleons (symbols) and quarks (lines). The vertical lines in each panel correspond to locations for 0.2%, 1% and 2% centralities.

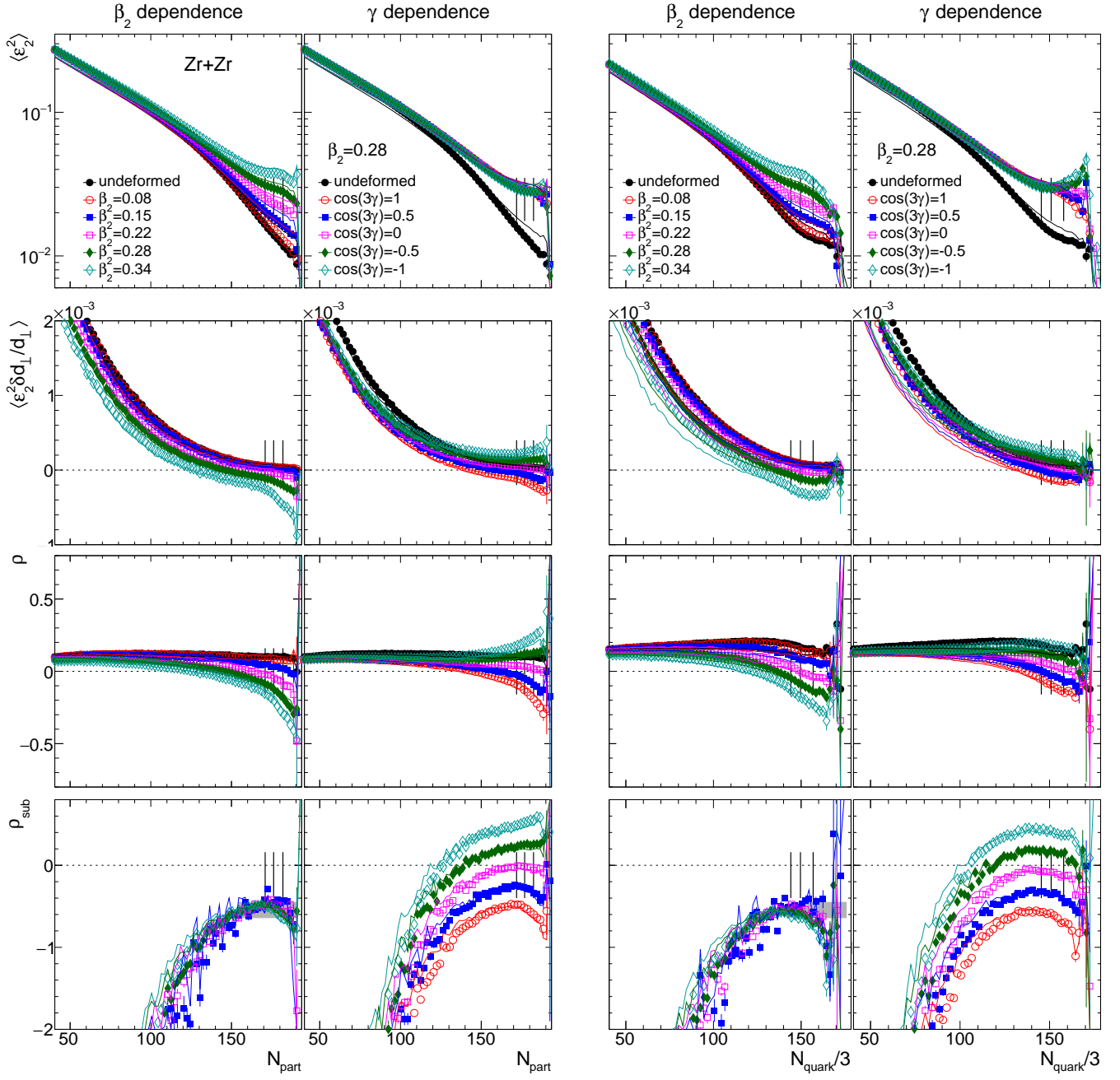


FIG. 21. Same as Fig. 20 but for Zr+Zr collisions.

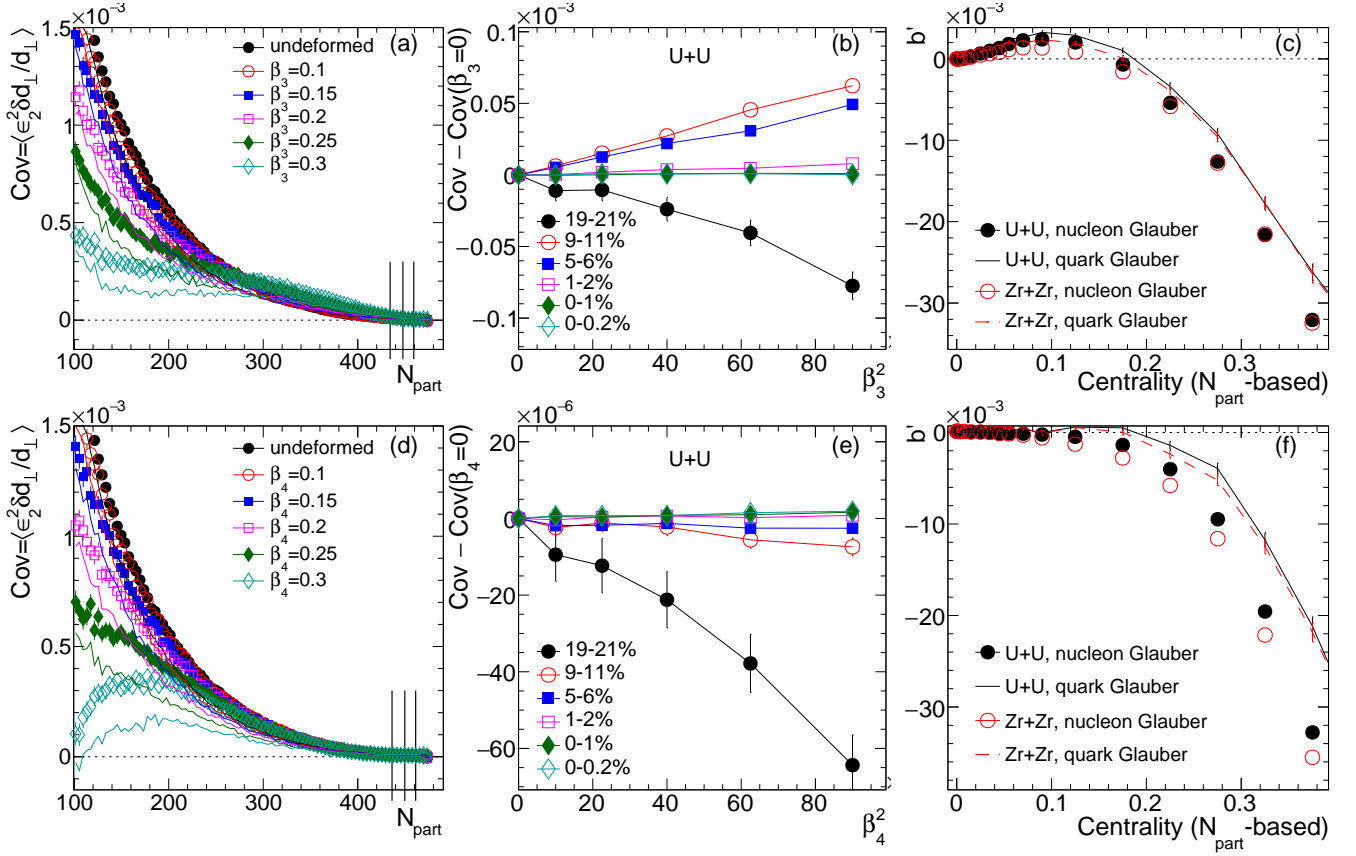


FIG. 22. The $\langle \varepsilon_2^2 \delta d_{\perp} / d_{\perp} \rangle$ for several values of β_3 (top row) and β_4 (bottom row) as a function of N_{part} (left column) or β_n^2 (middle column) in U+U collisions. The latter dependencies can be described by a simple $a' + b' \beta_n^2$ function. The right column summarizes the slope b' obtained from the middle panels as a function of centrality in U+U (black) and Zr+Zr (red) systems.

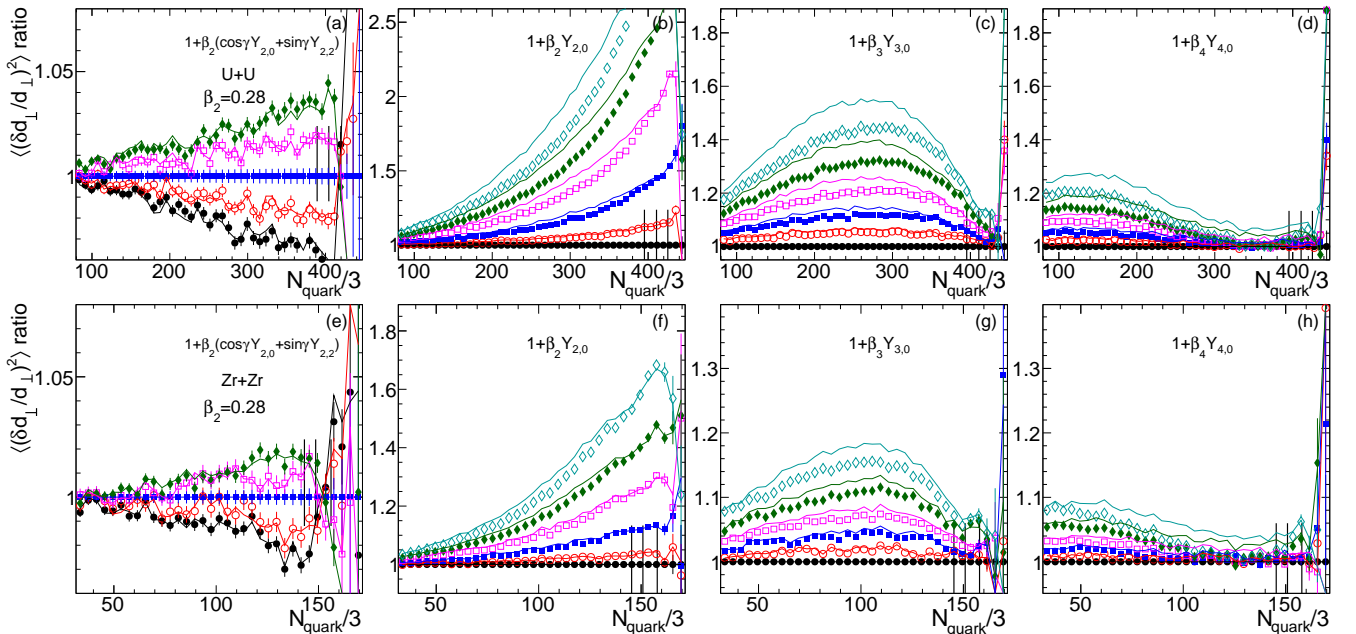


FIG. 23. Same as Fig. 5 in the main text, but event average is based on N_{quark} and plotted as a function of N_{quark} .

-
- [1] K. Heyde and J. L. Wood, Shape coexistence in atomic nuclei, *Rev. Mod. Phys.* **83**, 1467 (2011).
- [2] T. Togashi, Y. Tsunoda, T. Otsuka, and N. Shimizu, Quantum Phase Transition in the Shape of Zr isotopes, *Phys. Rev. Lett.* **117**, 172502 (2016), [arXiv:1606.09056 \[nucl-th\]](#).
- [3] K. Heyde and J. L. Wood, Nuclear shapes: from earliest ideas to multiple shape coexisting structures, *Phys. Scripta* **91**, 083008 (2016).
- [4] S. Frauendorf, Beyond the Unified Model, *Phys. Scripta* **93**, 043003 (2018), [arXiv:1710.01210 \[nucl-th\]](#).
- [5] S.-G. Zhou, Multidimensionally constrained covariant density functional theories—nuclear shapes and potential energy surfaces, *Phys. Scripta* **91**, 063008 (2016), [arXiv:1605.00956 \[nucl-th\]](#).
- [6] U. W. Heinz and A. Kuhlman, Anisotropic flow and jet quenching in ultrarelativistic U + U collisions, *Phys. Rev. Lett.* **94**, 132301 (2005), [arXiv:nucl-th/0411054](#).
- [7] P. Filip, R. Lednicky, H. Masui, and N. Xu, Initial eccentricity in deformed Au-197 + Au-197 and U-238 + U-238 collisions at $\sqrt{s_{NN}}=200$ GeV at the BNL Relativistic Heavy Ion Collider, *Phys. Rev. C* **80**, 054903 (2009).
- [8] Q. Y. Shou, Y. G. Ma, P. Sorensen, A. H. Tang, F. Videbæk, and H. Wang, Parameterization of Deformed Nuclei for Glauber Modeling in Relativistic Heavy Ion Collisions, *Phys. Lett. B* **749**, 215 (2015), [arXiv:1409.8375 \[nucl-th\]](#).
- [9] A. Goldschmidt, Z. Qiu, C. Shen, and U. Heinz, Collision geometry and flow in uranium + uranium collisions, *Phys. Rev. C* **92**, 044903 (2015), [arXiv:1507.03910 \[nucl-th\]](#).
- [10] G. Giacalone, J. Noronha-Hostler, M. Luzum, and J.-Y. Ollitrault, Hydrodynamic predictions for 5.44 TeV Xe+Xe collisions, *Phys. Rev. C* **97**, 034904 (2018), [arXiv:1711.08499 \[nucl-th\]](#).
- [11] G. Giacalone, Elliptic flow fluctuations in central collisions of spherical and deformed nuclei, *Phys. Rev. C* **99**, 024910 (2019), [arXiv:1811.03959 \[nucl-th\]](#).
- [12] G. Giacalone, J. Jia, and V. Somà, Accessing the shape of atomic nuclei with relativistic collisions of isobars, *Phys. Rev. C* **104**, L041903 (2021), [arXiv:2102.08158 \[nucl-th\]](#).
- [13] G. Giacalone, J. Jia, and C. Zhang, Impact of Nuclear Deformation on Relativistic Heavy-Ion Collisions: Assessing Consistency in Nuclear Physics across Energy Scales, *Phys. Rev. Lett.* **127**, 242301 (2021), [arXiv:2105.01638 \[nucl-th\]](#).
- [14] J. Jia, S. Huang, and C. Zhang, Probing nuclear quadrupole deformation from correlation of elliptic flow and transverse momentum in heavy ion collisions, *Phys. Rev. C* **105**, 014906 (2022), [arXiv:2105.05713 \[nucl-th\]](#).
- [15] J. Jia, Shape of atomic nuclei in heavy ion collisions, *Phys. Rev. C* **105**, 014905 (2022), [arXiv:2106.08768 \[nucl-th\]](#).
- [16] B. Bally, M. Bender, G. Giacalone, and V. Somà, Evidence of the triaxial structure of ^{129}Xe at the Large Hadron Collider, *Phys. Rev. Lett.* **128**, 082301 (2022), [arXiv:2108.09578 \[nucl-th\]](#).
- [17] L. Adamczyk *et al.* (STAR), Azimuthal anisotropy in U+U and Au+Au collisions at RHIC, *Phys. Rev. Lett.* **115**, 222301 (2015), [arXiv:1505.07812 \[nucl-ex\]](#).
- [18] ALICE Collaboration, Anisotropic flow in Xe-Xe collisions at $\sqrt{s_{NN}} = 5.44$ TeV, *Phys. Lett. B* **784**, 82 (2018), [arXiv:1805.01832 \[nucl-ex\]](#).
- [19] A. M. Sirunyan *et al.* (CMS), Charged-particle angular correlations in XeXe collisions at $\sqrt{s_{NN}} = 5.44$ TeV, *Phys. Rev. C* **100**, 044902 (2019), [arXiv:1901.07997 \[hep-ex\]](#).
- [20] G. Aad *et al.* (ATLAS), Measurement of the azimuthal anisotropy of charged-particle production in Xe + Xe collisions at $\sqrt{s_{NN}} = 5.44$ TeV with the ATLAS detector, *Phys. Rev. C* **101**, 024906 (2020), [arXiv:1911.04812 \[nucl-ex\]](#).
- [21] J. Jia, Nuclear deformation effects via Au+Au and U+U collisions from STAR, Contribution to the VIth International Conference on the Initial Stages of High-Energy Nuclear Collisions, January 2021, <https://indico.cern.ch/event/854124/contributions/4135480/> (2021).
- [22] A. Bohr and B. R. Mottelson, eds., *Nuclear Structure* (World Scientific, 1998).
- [23] S. Frauendorf and N. Jie Meng, Tilted rotation of triaxial nuclei, *Nucl. Phys. A* **617**, 131 (1997).
- [24] S. W. Ødegård, G. B. Hagemann, D. R. Jensen, M. Bergström, B. Herskind, G. Sletten, S. Törmänen, J. N. Wilson, P. O. Tjøm, I. Hamamoto, K. Spohr, H. Hübel, A. Görge, G. Schönwasser, A. Bracco, S. Leoni, A. Maj, C. M. Petrache, P. Bednarczyk, and D. Curien, Evidence for the wobbling mode in nuclei, *Phys. Rev. Lett.* **86**, 5866 (2001).
- [25] S. Frauendorf, Spontaneous symmetry breaking in rotating nuclei, *Rev. Mod. Phys.* **73**, 463 (2001).
- [26] W. Busza, K. Rajagopal, and W. van der Schee, Heavy Ion Collisions: The Big Picture, and the Big Questions, *Ann. Rev. Nucl. Part. Sci.* **68**, 339 (2018), [arXiv:1802.04801 \[hep-ph\]](#).
- [27] U. W. Heinz, Towards the Little Bang Standard Model, *J. Phys. Conf. Ser.* **455**, 012044 (2013), [arXiv:1304.3634 \[nucl-th\]](#).
- [28] P. Bożek and W. Broniowski, Transverse-momentum fluctuations in relativistic heavy-ion collisions from event-by-event viscous hydrodynamics, *Phys. Rev. C* **85**, 044910 (2012), [arXiv:1203.1810 \[nucl-th\]](#).
- [29] B. Schenke, C. Shen, and D. Teaney, Transverse momentum fluctuations and their correlation with elliptic flow in nuclear collision, *Phys. Rev. C* **102**, 034905 (2020), [arXiv:2004.00690 \[nucl-th\]](#).
- [30] H. Niemi, K. J. Eskola, and R. Paatelainen, Event-by-event fluctuations in a perturbative QCD + saturation + hydrodynamics model: Determining QCD matter shear viscosity in ultrarelativistic heavy-ion collisions, *Phys. Rev. C* **93**, 024907 (2016), [arXiv:1505.02677 \[hep-ph\]](#).
- [31] D. Teaney and L. Yan, Non linearities in the harmonic spectrum of heavy ion collisions with ideal and viscous hydrodynamics, *Phys. Rev. C* **86**, 044908 (2012), [arXiv:1206.1905 \[nucl-th\]](#).
- [32] J. E. Bernhard, J. S. Moreland, S. A. Bass, J. Liu, and U. Heinz, Applying Bayesian parameter estimation to relativistic heavy-ion collisions: simultaneous characterization of the initial state and quark-gluon plasma medium, *Phys. Rev. C* **94**, 024907 (2016), [arXiv:1605.03954 \[nucl-th\]](#).

- [33] J. E. Bernhard, J. S. Moreland, and S. A. Bass, Bayesian estimation of the specific shear and bulk viscosity of quark–gluon plasma, *Nature Phys.* **15**, 1113 (2019).
- [34] G. Nijs, W. van der Schee, U. Gürsoy, and R. Snellings, A transverse momentum differential global analysis of Heavy Ion Collisions, *Phys. Rev. Lett.* **126**, 202301 (2021), arXiv:2010.15130 [nucl-th].
- [35] G. Giacalone, Observing the deformation of nuclei with relativistic nuclear collisions, *Phys. Rev. Lett.* **124**, 202301 (2020), arXiv:1910.04673 [nucl-th].
- [36] Y. Alhassid, C. N. Gilbreth, and G. F. Bertsch, Nuclear deformation at finite temperature, *Phys. Rev. Lett.* **113**, 262503 (2014), arXiv:1408.0081 [nucl-th].
- [37] P. Bozek, Transverse-momentum–flow correlations in relativistic heavy-ion collisions, *Phys. Rev. C* **93**, 044908 (2016), arXiv:1601.04513 [nucl-th].
- [38] M. L. Miller, K. Reygers, S. J. Sanders, and P. Steinberg, Glauber modeling in high energy nuclear collisions, *Ann. Rev. Nucl. Part. Sci.* **57**, 205 (2007), arXiv:nucl-ex/0701025.
- [39] S. S. Adler *et al.* (PHENIX), Transverse-energy distributions at midrapidity in p+p, d+Au, and Au+Au collisions at $\sqrt{s_{NN}} = 62.4\text{--}200$ GeV and implications for particle-production models, *Phys. Rev.* **C89**, 044905 (2014), arXiv:1312.6676 [nucl-ex].
- [40] R. A. Lacey, P. Liu, N. Magdy, M. Csanád, B. Schweid, N. N. Ajitanand, J. Alexander, and R. Pak, Scaling properties of the mean multiplicity and pseudorapidity density in $e^- + e^+$, $e^\pm + p$, $p(\bar{p}) + p$, p+A and A+A(B) collisions, *Universe* **4**, 22 (2018), arXiv:1601.06001 [nucl-ex].
- [41] C. Loizides, Glauber modeling of high-energy nuclear collisions at the subnucleon level, *Phys. Rev.* **C94**, 024914 (2016), arXiv:1603.07375 [nucl-ex].
- [42] P. Bożek, W. Broniowski, and M. Rybczyński, Wounded quarks in A+A, p+A, and p+p collisions, *Phys. Rev.* **C94**, 014902 (2016), arXiv:1604.07697 [nucl-th].
- [43] S. Acharya *et al.* (ALICE), Centrality and pseudorapidity dependence of the charged-particle multiplicity density in Xe–Xe collisions at $\sqrt{s_{NN}} = 5.44$ TeV, *Phys. Lett.* **B790**, 35 (2019), arXiv:1805.04432 [nucl-ex].
- [44] V. Skokov, B. Friman, and K. Redlich, Volume Fluctuations and Higher Order Cumulants of the Net Baryon Number, *Phys. Rev.* **C88**, 034911 (2013), arXiv:1205.4756 [hep-ph].
- [45] M. Zhou and J. Jia, Centrality fluctuations in heavy-ion collisions, *Phys. Rev. C* **98**, 044903 (2018), arXiv:1803.01812 [nucl-th].
- [46] M. Aaboud *et al.* (ATLAS), Fluctuations of anisotropic flow in Pb+Pb collisions at $\sqrt{s_{NN}} = 5.02$ TeV with the ATLAS detector, *JHEP* **01**, 051, arXiv:1904.04808 [nucl-ex].
- [47] J. T. Mitchell, D. V. Perepelitsa, M. J. Tannenbaum, and P. W. Stankus, Tests of constituent-quark generation methods which maintain both the nucleon center of mass and the desired radial distribution in Monte Carlo Glauber models, *Phys. Rev.* **C93**, 054910 (2016), arXiv:1603.08836 [nucl-ex].
- [48] T. De Forest, Jr. and J. D. Walecka, Electron scattering and nuclear structure, *Adv. Phys.* **15**, 1 (1966).
- [49] G.-L. Ma and Z.-W. Lin, Predictions for $\sqrt{s_{NN}} = 5.02$ TeV Pb+Pb Collisions from a Multi-Phase Transport Model, *Phys. Rev. C* **93**, 054911 (2016), arXiv:1601.08160 [nucl-th].
- [50] P. A. Butler, Octupole collectivity in nuclei, *J. Phys. G* **43**, 073002 (2016).
- [51] M. Abdallah *et al.* (STAR), Search for the chiral magnetic effect with isobar collisions at $\sqrt{s_{NN}} = 200$ GeV by the STAR Collaboration at the BNL Relativistic Heavy Ion Collider, *Phys. Rev. C* **105**, 014901 (2022), arXiv:2109.00131 [nucl-ex].
- [52] ATLAS Collaboration, *Measurement of flow and transverse momentum correlations in Pb+Pb collisions at $\sqrt{s_{NN}} = 5.02$ TeV and Xe+Xe collisions at $\sqrt{s_{NN}} = 5.44$ TeV with the ATLAS detector*, Tech. Rep. (CERN, Geneva, 2021).
- [53] J. Jia and C.-J. Zhang, Scaling approach to nuclear structure in high-energy heavy-ion collisions, arXiv:2111.15559 [nucl-th] (2021).
- [54] C. Zhang and J. Jia, Evidence of Quadrupole and Octupole Deformations in Zr96+Zr96 and Ru96+Ru96 Collisions at Ultrarelativistic Energies, *Phys. Rev. Lett.* **128**, 022301 (2022), arXiv:2109.01631 [nucl-th].
- [55] P. Bożek, W. Broniowski, and S. Chatterjee, Transverse Momentum Fluctuations and Correlations, *Acta Phys. Polon. Supp.* **10**, 1091 (2017), arXiv:1707.04420 [nucl-th].
- [56] G. Giacalone, F. G. Gardim, J. Noronha-Hostler, and J.-Y. Ollitrault, Correlation between mean transverse momentum and anisotropic flow in heavy-ion collisions, *Phys. Rev. C* **103**, 024909 (2021), arXiv:2004.01765 [nucl-th].
- [57] Z.-W. Lin, C. M. Ko, B.-A. Li, B. Zhang, and S. Pal, A Multi-phase transport model for relativistic heavy ion collisions, *Phys. Rev. C* **72**, 064901 (2005), arXiv:nucl-th/0411110.
- [58] J. Xu and C. M. Ko, Higher-order anisotropic flows and dihadron correlations in Pb-Pb collisions at $\sqrt{s_{NN}} = 2.76$ TeV in a multiphase transport model, *Phys. Rev.* **C84**, 044907 (2011), arXiv:1108.0717 [nucl-th].
- [59] J. Xu and C. M. Ko, Triangular flow in heavy ion collisions in a multiphase transport model, *Phys. Rev.* **C84**, 014903 (2011), arXiv:1103.5187 [nucl-th].
- [60] C. Zhang, L. Zheng, S. Shi, and Z.-W. Lin, Using local nuclear scaling of initial condition parameters to improve the system size dependence of transport model descriptions of nuclear collisions, *Phys. Rev. C* **104**, 014908 (2021), arXiv:2103.10815 [nucl-th].
- [61] J. Adam *et al.* (STAR), Collision-energy dependence of p_t correlations in Au + Au collisions at energies available at the BNL Relativistic Heavy Ion Collider, *Phys. Rev. C* **99**, 044918 (2019), arXiv:1901.00837 [nucl-ex].
- [62] G. Giacalone, F. G. Gardim, J. Noronha-Hostler, and J.-Y. Ollitrault, Skewness of mean transverse momentum fluctuations in heavy-ion collisions, *Phys. Rev. C* **103**, 024910 (2021), arXiv:2004.09799 [nucl-th].
- [63] G.-L. Ma and A. Bzdak, Long-range azimuthal correlations in proton–proton and proton–nucleus collisions from the incoherent scattering of partons, *Phys. Lett.* **B739**, 209 (2014), arXiv:1404.4129 [hep-ph].

- [64] A. Bzdak and G.-L. Ma, Elliptic and triangular flow in p +Pb and peripheral Pb+Pb collisions from parton scatterings, *Phys. Rev. Lett.* **113**, 252301 (2014), [arXiv:1406.2804 \[hep-ph\]](#).
- [65] M.-W. Nie, P. Huo, J. Jia, and G.-L. Ma, Multiparticle azimuthal cumulants in p +Pb collisions from a multiphase transport model, *Phys. Rev.* **C98**, 034903 (2018), [arXiv:1802.00374 \[hep-ph\]](#).
- [66] C. Zhang, A. Behera, S. Bhatta, and J. Jia, Non-flow effects in correlation between harmonic flow and transverse momentum in nuclear collisions, *Phys. Lett. B* **822**, 136702 (2021), [arXiv:2102.05200 \[nucl-th\]](#).
- [67] H. Song, S. A. Bass, U. Heinz, T. Hirano, and C. Shen, 200 A GeV Au+Au collisions serve a nearly perfect quark-gluon liquid, *Phys. Rev. Lett.* **106**, 192301 (2011), [Erratum: *Phys.Rev.Lett.* 109, 139904 (2012)], [arXiv:1011.2783 \[nucl-th\]](#).